Original Paper

Modification of the cation exchange population and CEC values of reacted bentonites of the third retrieved package of the alternative buffer material (ABM-5) experiment operated at up to 250°C

R. Dohrmann[1,2] ⓘ, J. Gröger-Trampe[1] and S. Kaufhold[2] ⓘ

[1]State Authority of Mining, Energy and Geology (LBEG), Stilleweg 2, D-30655 Hannover, Germany and [2]Federal Institute for Geosciences and Natural Resources (BGR), Stilleweg 2, D-30655 Hannover, Germany

Abstract

Cation exchange competition (CEC) is driven by water uptake during saturation of bentonite barriers surrounding canisters releasing heat from radioactive waste. CEC differences may be used to follow smectite degradation. The unanswered question is whether processes can be understood in more detail by studying a full set of 30 bentonite blocks of the Alternative Buffer Material (ABM) test series (ABM-5) after reaction in an underground laboratory operated in crystalline rock at temperatures of ~250°C, the highest reported temperature so far. In contrast to expectations, only a minor CEC decrease of, on average, 1.8 meq 100 g^{-1} was detected, although processes depending on high temperature were expected to alter the swelling properties of smectites that can be followed analytically by reducing bentonite CEC values. A critical role of initial water saturation and initially ~25% Na$^+$/CEC on exchangers was identified by comparison with the first ABM-1 package where CEC decreased by on, average, 5.5 meq 100 g^{-1}. ABM-1 was heated from the start whereas the packages ABM-2 and ABM-5 in this study were heated after water saturation. Exchangeable cations (EC) were distributed within the whole barrier in ABM-5 with (1) more pronounced horizontal EC gradients and (2) the absence of an exchangeable Na$^+$ decrease. In all tests, a cation equilibration with the Äspö groundwater averaged over the whole packages of many different buffer materials was observed, showing, overall, a significant range in final composition after retrieval: Na$^+$ (27–46%/CEC), Mg^{2+} (7–15%/CEC), and Ca^{2+} (45–100%/CEC). The groundwater for saturation, however, was locally variable in composition. Although excluded from the smectite interlayer (below or equal to 2 water layers), Cl$^-$ entered the barrier from groundwater, increased significantly in nearly all ABM-5 bentonite blocks, and was found to be mobile also in the less heated ABM-1 and ABM-2 test packages.

Keywords: bentonite buffer; CEC; Cu-trien5xcalcite; exchangeable cation population

Introduction

In many countries, high-level radioactive waste (HLRW) will be stored in deep geological disposal facilities made of either crystalline rock, clay rock formations, or rock salt. In concepts with crystalline rock, bentonites are candidate materials for encapsulation of the canisters containing heat-developing waste, and their primary functions are sorption and swelling capacity, low hydraulic conductivity, etc. (Faucher et al., 1952; Gaines and Thomas, 1953; Neretnieks, 1978; Jacobsson and Pusch, 1978; Sellin and Leupin, 2014). Smectites are the main minerals of bentonites used in such an application and numerous studies have focused on long-term stability of the barrier materials in such systems.

As outlined by Bildstein and Claret (2015), clay barriers 'react due to changes in the initial physicochemical conditions (pH and redox potential, aqueous species concentrations) and/or the introduction of 'foreign' materials (iron, steel, concrete, glass, bitumen, etc.)'. In principle, barrier stability studies can be conducted in clay laboratories, in underground rock laboratories, or in natural analogue studies (e.g. Dohrmann et al., 2013a). An important factor is the water/rock (or liquid/solid) ratio, which is usually unrealistically large in laboratory studies when, for example, slurries are used in batch experiments to mimic highly compacted bentonite blocks. On the other hand, many different test series can be conducted in the laboratory to find differences, such as different bentonite materials or different test parameters such as temperature, electrolyte concentration, or density (degree of compaction) (e.g. Kaufhold and Dohrmann, 2016).

The strength of natural analogue (NA) studies is the time factor, which allows us to learn about long-term processes affecting barrier stability with respect to factors such as heat and alkaline perturbation. Pusch (1983) and Brusewitz (1986) described mineralogical changes in Ordovician bentonite layers in Kinnekulle, Sweden. Those authors attempted to discover if heat caused by an intrusion may have generated loss of swelling capacity of smectitic layers due to illitization and release of free silica (cf. Kaufhold et al., 2023a). Temperatures >100°C from the resulting heat plume influenced the bentonite layer for several hundreds of years. Even such long reaction times were not sufficient to clarify whether real illitization processes were present as argued by Müller-Vonmoos et al. (1990, 1994), who studied the same bentonite beds and did not agree with the suggestion that smectites in these bentonites were transformed to illite. Alteration of bentonites by alkaline solutions (from cement used as the barrier component) is of concern and well documented in NA studies (e.g. Savage, 2011; Shimbashi et al., 2024).

Loss of swelling capacity due to illitization remains an important question for long-term safety evaluation. If alteration processes such as illitization of smectite are limited to long reaction times, increasing other parameters such as reaction temperature is a way to obtain information on the risk of illitization in underground rock laboratory experiments. Such *in situ* experiments in underground rock laboratories require a certain effort for installation of materials that can require the drilling of a gallery 100 m long, which is costly. On the other hand, the final materials to be sampled are then altered under more realistic boundary conditions compared with typical laboratory experiments.

The maximum temperature of the geotechnical HLRW bentonite barrier and effects of heat on barrier integrity are still the subject of debate (e.g. Zheng et al., 2015; Sun et al., 2022; Kaufhold et al., 2023a). *In situ* experiments at temperatures >100°C were conducted in the hard rock laboratory in Äspö, Sweden, to evaluate whether canister surface temperatures may alter the bentonite barrier material: The 'Long Term Test of Buffer Materials' (LOT) (Karnland et al., 2000; Olsson and Karnland, 2011), the 'Temperature Buffer Test' experiment (TBT) (Sandén et al., 2007), and the 'Alternative Buffer Material test' (ABM) (Eng et al., 2007; Sandén et al., 2018). In LOT and TBT, Wyoming-type bentonite (brand name MX80) compacted to bentonite blocks was used with a heater (made of copper) in the center. In ABM experiments, different buffer materials were used. In ABM-1 to -3 these were mostly bentonite, plus claystones and granular materials inserted in cages. In ABM-4 (not yet studied) and ABM-5, only bentonites were used. In all ABM experiments, buffer materials had various exchangeable cation (EC) populations and all buffer materials were packed vertically on each other with an iron tube as heater in the center.

During heating, groundwater is expected to enter the blocks, slowly saturating the bentonite buffer materials by diffusion from the rock side to the heater. This causes cation exchange to be the first observable geochemical reaction as modeled by Arcos et al. (2000) and confirmed by analyzing material from the LOT experiment in which Na^+ was exchanged by Ca^{2+} and Mg^{2+}. In addition, Cl^- and SO_4^{2-} concentrations increased (Karnland et al., 2009). The set-up of ABM with many different materials with different starting (reference) exchangeable cation (EC) compositions allowed evaluation on a larger scale. In samples of ABM-1 heated to 140°C maximum and studied after retrieval of the package by Kumpulainen and Kiviranta (2011) (4 blocks), Svensson et al. (2011) (11 blocks), and Dohrmann et al. (2013b) (21 blocks), such distribution over the entire package for the whole EC population ($EC_{population}$) was confirmed after a reaction time of just 1 year.

A similar but even stronger interaction of Äspö groundwater with the buffer materials used was expected for ABM-2, as this was heated for 4.5 years. Kumpulainen et al. (2016) studied cation exchange of four blocks in the lowest part of the experiment and Dohrmann and Kaufhold (2017) studied all 31 blocks except for two (these two blocks had disintegrated and could not be sampled properly). Again, significant modification of the $EC_{population}$ was reported and particularly large amounts of Ca^{2+} were extracted in the cation exchange competition (CEC) experiments with parts of that Ca^{2+} being a signature of the groundwater greatly exceeding the total CEC. Dohrmann and Kaufhold (2017) concluded that anhydrite formation confirmed groundwater as the Ca^{2+} source. The authors described disintegration of many blocks and concluded that boiling possibly occurred in the warmest part of the experiment, causing the observed disintegration. Svensson et al. (2023) discussed additional findings such as formation of halite and confirmed that boiling possibly occurred in ABM-2. Svensk Kärnbränslehantering AB (SKB, Sweden) started a new experiment series of ABM called ABM-45 (Sandén et al., 2018) which was made of only bentonite blocks. These 12 bentonites included three bentonites that were not used in other ABM tests previously. ABM-5 was the first of these experiments that was terminated after being heated to 250°C, and it was the third ABM package to be sampled.

ABM-5 was dismantled in 2017. It was the third excavated parcel after ABM-1 and ABM-2 (first phase of the project). ABM-5 blocks had been heated in three steps starting with: (1) a 2.5-year phase at ~50°C; (2) a 4-month phase of up to 132°C; followed by (3) a 7-month phase of up to 250°C (Fig. 1) (Sandén et al., 2018).

Cation exchange in the investigated heater tests was fast and significant. Different trends were observed when comparing cation exchange found in ABM-1 and ABM-2, which means that no specific exchange pattern was observed, either depending on the materials used or on specific temperature. The conclusion thus far was that locally varying conditions within the bentonite block packages may have caused the locally different exchange patterns, including locally different temperature (gradients) and also fractures in crystalline rock with increased groundwater inflow in the sand filters surrounding the packages. Because of the high temperature applied in the ABM-5 test, this test was considered to be particularly suitable for studying a possible specific effect of the temperature on the cation exchange pattern.

The aims of the study were, therefore, to find out: (1) if heating to 250°C caused differences in $EC_{population}$ with respect to equilibrium of ECs over the entire package as already observed for ABM-1 and ABM-2; (2) if high temperatures may have affected equilibria between exchangeable cations as observed for ABM-1 and ABM-2 with a pronounced loss of exchangeable Na^+ and Mg^{2+}; (3) if high temperatures may also have caused a reduction in CEC resulting either from illitization or irreversible interlayer collapse; and (4) if chloride was distributed in the package as observed previously in both ABM-1 and ABM-2.

Materials and methods

ABM design

The ABM experiment was designed based on the Swedish KBS-3 concept with a metal canister surrounded by clay situated in crystalline bedrock at a depth of ~500 m (Eng et al., 2007; SKB, 2007). The maximum temperature was designed to be >100°C in the ABM buffer differing from the reference case and hence from the real scale prototype repository *in situ* experiment (PR) conditions
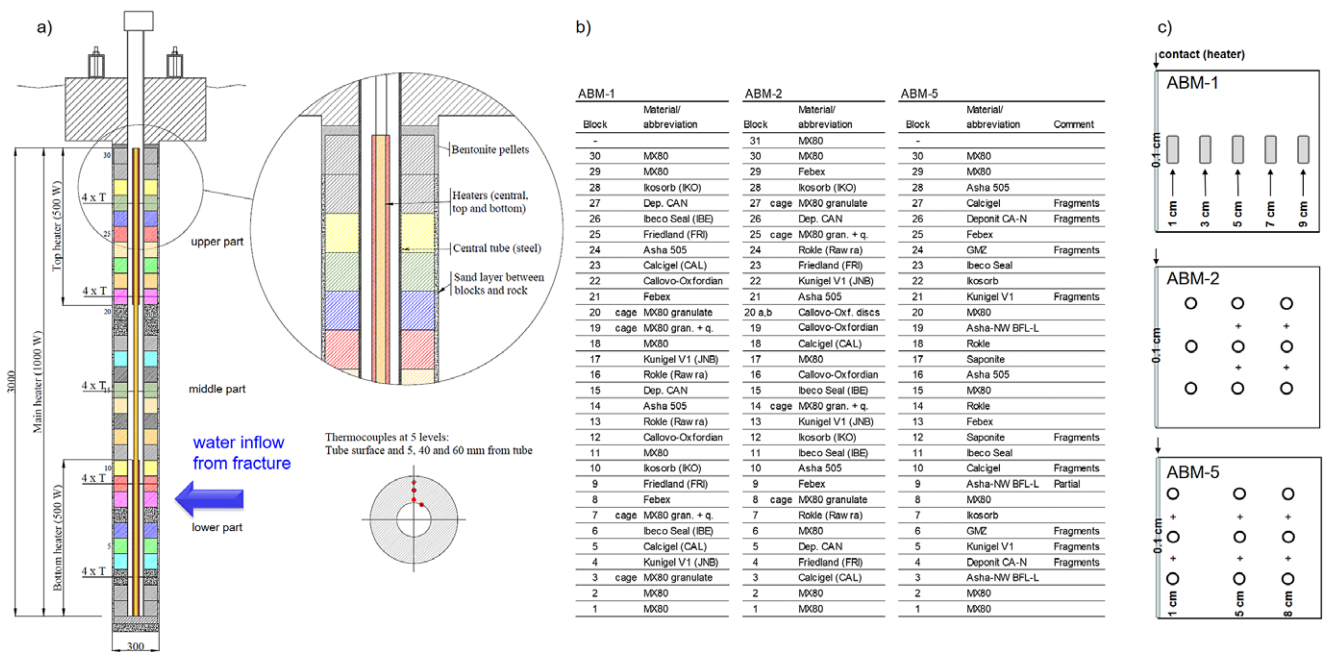
Figure 1. Diagram of the ABM packages showing the positions of: (a) the thermocouples (4T) and heaters, taken from Sandén et al. (2018); (b) the block order in the ABM-1, ABM-2, and ABM-5 (present study) packages; and (c) the sampling schemes. The following blocks were fractured and could not be sampled at all distances of 1 cm, 5 cm, 8 cm: #3, #4, #6, #92, #24, #27.

(Johannesson et al., 2007; Dohrmann and Kaufhold, 2014). Similar to the LOT *in situ* experiment (Olsson and Karnland, 2011), the ABM was installed as an intermediate-scale experiment (1:4) and in contrast to other experiments at Äspö, different buffer materials were used, and common carbon steel (P235TR1) was used as the canister metal instead of copper (Table 1). With increased combinations of materials in contact with carbon steel, corrosion and processes initiated by corrosion, water saturation, and high temperatures were expected (Wersin and Birgersson, 2014; Wersin et al., 2015; Kaufhold et al., 2015; Samper et al., 2016; Kaufhold et al., 2017a) and this also allowed us to compare the corrosion effects with those of the copper/bentonite interface (Szakálos and Seetharaman, 2012; Kosec et al., 2015; Kaufhold et al., 2017b; Kaufhold et al., 2023a). Both sets of ABM experiments (Eng et al., 2007; Sandén et al., 2018) were installed in boreholes in crystalline rock with a diameter of 300 mm and a depth of 3 m (Fig. 1). ABM-1 to -3 test series were installed in 2006 and the second test series, called ABM-45, was installed in 2012 (Svensson et al., 2023) in a separate niche of the laboratory. The outer diameter of the ring blocks was 280 mm, the inner diameter was 110 mm, and the height of the individual ring blocks was 100 mm. In each of the ABM experimental packages, three electrical heaters were installed to yield the target temperature in the bentonite blocks with a main heater along the entire package length (Fig. 1) and two additional heaters at the bottom and at the top for a more homogeneous temperature distribution in the buffer materials. Temperatures varied within the blocks and were up to almost 100°C warmer at the bentonite/heater interface than at the bentonite/rock interface (Svensson et al., 2023). Up until now, three ABM packages have been excavated and analyzed: ABM-1, ABM-2, and ABM-5. The duration of ABM-2 and ABM-5 experiments can be split into two phases each, one with water saturation followed by stepwise heating (Svensson et al., 2023); whereas ABM-1 was heated from the start without waiting several months to detect full water saturation by relative humidity sensors installed in the bentonite materials.

In contrast to the initial packages, ABM-1 to -3, in ABM-5 only different bentonite buffer materials were packed on top of each other leaving out marine clay rocks and cages with granular buffer/backfill mixtures used in ABM-1 and ABM-2, respectively. The denotations/abbreviations, and origins of the bentonites with three new materials were: Asha NW BFL-L (Asha NW, India), Geohellas saponite (Greece), and GMZ (Chinese reference material, China).

Table 1. Experimental parameters of important projects for assessment of bentonite buffers in various underground or hard rock laboratories

Experiment	HRL/URL	Metal (heater)	Host rock	T (max)	Salinity (groundwater)	Scale
LOT	Äspö	copper	crystalline	ca. 140°C	high (Na-Ca-Cl-SO$_4$)	intermediate scale
ABM–1	Äspö	iron	crystalline	ca. 140°C	high (Na-Ca-Cl-SO$_4$)	intermediate scale
ABM–2	Äspö	iron	crystalline	ca. 140°C	high (Na-Ca-Cl-SO$_4$)	intermediate scale
ABM–5	Äspö	iron	crystalline	ca. 250°C	high (Na-Ca-Cl-SO$_4$)	intermediate scale
Prototype Repository	Äspö	copper	crystalline	ca. 85°C	high (Na-Ca-Cl-SO$_4$)	full scale
FEBEX-DP	Grimsel	iron	crystalline	ca. 100°C	low (Na-Ca-HC0$_3$-F)	full scale
Heater B	Mont Terri	iron	clay	ca. 100°C	Mont Terri pore water	intermediate scale

The bentonite referred to as 'Saponite' is rich in the smectite-group mineral saponite (trioctahedral). In order to avoid misinterpretation, the bentonite is labelled 'Saponite' in this study to distinguish it from the mineral. On the other hand, nine identical labeled materials were used, as in ABM-1 and ABM-2: MX80 (important reference material in crystalline rock concepts, Wyoming, USA), Kunigel V1 (Japanese reference material, JNB, Tsukinuno, Japan), Calcigel (CAL, Bavaria, Germany), Ikosorb (IKO, Mount Tidienit, Morocco), Rokle (Rokle, Czech Republic), Asha 505 (India), Deponit CAN (Dep. CAN, Milos, Greece), Febex (Spanish reference material, Almeria, Spain), and Ibeco Seal (Ibeco Seal M-90 IBE, Askana, Georgia/CIS).

The Ibeco Seal bentonite used in ABM-5, however, had an identical brand name but was from another charge of raw materials (table 5-1 in Sandén et al., 2018) with a different composition. This can be followed by comparing reference data differences (X-ray fluorescence (XRF) chemical composition, CEC, and EC data) of the ABM-1 and ABM-2 IBE materials compared with reference material recently published for ABM-5 Ibeco Seal materials (Fernández et al., 2022). ABM-5 Ibeco Seal had approximately the same CEC values, but three times as much exchangeable Na^+, along with ~50% less Ca^{2+} and Mg^{2+}. If not explicitly mentioned, in this study Ibeco Seal was used only for the ABM-5 Ibeco Seal material. Febex bentonites were also from two different batches but the samples were more or less identical in composition (Fernández et al., 2022).

After compaction into rings, bentonite blocks were positioned on top of each other, encapsulating the tube. The first block from the bottom is positioned on a bottom plate made of the same steel as the tube and welded to the tube, whereas the top block is covered with bentonite pellets followed by a concrete lid towards the gallery. All reference (REF) materials were installed twice in the test package, except for MX80 bentonite (seven times) and Asha NW BFL-L (three times), and all but the MX80 were separated by other blocks (Fig. 1). The $EC_{population}$ values in the various REF materials were significantly different.

After emplacement of the ABM packages, a slot ~10 mm thick between the package and the rock was filled with sand to allow inflowing groundwater to be distributed uniformly around the bentonite rings. In contrast to the installation plan, in ABM-5 groundwater was only added by natural inflow from the rock into the test hole whereas the artificial water saturation system that was also installed in ABM-1 and ABM-2 with perforated titanium pipes aimed to supply the bentonite blocks with water from a tank in the gallery above the packages was more or less unused. The reason was that the inflow to the ABM-5 hole was so great that 5 days after having cast the concrete lid and mounted the steel beams, only 2 L of water was injected into the ABM-5 tests before water started to leak out on the floor, indicating that the sand filter was already filled up with water from the fracture identified earlier. As the fracture had connections to the floor and because it was not possible to apply water pressure in the filter, water injection into ABM-5 was closed and was not used thereafter (Svensson et al., 2023). Because of these pressure problems in the fracture, ABM-5 was first allowed to saturate with water for ~2.5 years. After closing the connection to the artificial water-saturation system, the package was heated at two different temperatures for ~4 months (132°C maximum) and 7 months (250°C maximum).

The nearly-neutral pH Äspö water present in the niche of this project (Dueck et al., 2011) used for natural saturation was a Na-Ca-Cl-dominated groundwater (~1600 mg L^{-1} Na^+ and 760 mg L^{-1} Ca^{2+}, ~3970 mg L^{-1} Cl^-, and ~330 mg L^{-1} SO_4^{2-}) with minor amounts of Mg^{2+}, Br^-, and K^+ (all <120 mg L^{-1}). The salinity of the groundwater was much less than in the first three ABM packages (ABM-1,

ABM-2, and ABM-3) which were installed in another niche in the hard rock laboratory.

Upon dismantling of the ABM-5 package, some of the blocks were found to be more fragile than in the ABM-1 package and thus could not be sampled as planned (with defined distances to the heater). Large fractures ran along the entire package in the bentonite with some intact blocks, while others were highly fractured and very fragile, probably due to the high temperature applied (Svensson et al., 2023) (Fig. 2).

The temperature distribution, as expected, was not homogeneous and the peak temperatures were recorded by sensors in the buffer at a few centimeters from the heater. Even in the outer part, maximum temperatures of ~150°C were recorded (Fig. 2c), exceeding maximum temperatures observed in most other experiments performed in underground or hard rock laboratories (Table 1).

The ABM-5 was sampled in our laboratory and all blocks were analyzed for mineralogical/geochemical changes (Kaufhold et al., 2021) and particularly for ion-exchange reactions (this study). In the literature, several ABM-5 blocks have been analyzed already. Most of the geochemical and mineralogical alterations of the different reacted ABM-5 bentonites (apart from the ECs) were restricted to the contacts between the iron heater and the bentonite as reported for sliced samples of five blocks (Kumar et al., 2021), 30 blocks (Kaufhold et al., 2021), five blocks (Fernández et al., 2022), and four blocks (Svensson et al., 2023). No cation exchange processes in any of these blocks were examined in those studies, however. $EC_{population}$ data so far are only available for a couple of blocks. The present study was designed to give information about overall changes in CECs and the $EC_{population}$ values of the whole package. To reach this goal, all blocks were investigated, essential to understanding the processes that occurred in ABM-5.

Sampling

After excavation, the blocks were sampled at various distances from the contact to the iron tube (Fig. 1), allowing study of horizontal variations in the buffer materials between the heater and the rock. A minimum of 2 g of material was required to perform the analytical work needed for this study and exactly the same samples were used by Kaufhold et al. (2021). Some blocks were intact, and some were partly disintegrated. In order to collect 2 g of material at a horizontal distance of 2 cm from the heater, three holes at 2 cm distance each were drilled and materials were mixed together in order to obtain an overview of the whole block thickness. If blocks were partly disintegrated, the sample mass was collected using more than three holes at the same distance. This procedure was repeated for samples at 5 cm and 8 cm (cf. Fig. 1c). The block pieces could not be sampled uniformly because some were fragmented, as shown in Fig. 1c. Therefore, any possible vertical gradients that might have occurred within single blocks could not be investigated based on this sample set. Excavation of any of the ABM experiments could not be performed in an O_2-free atmosphere and, therefore, no glove box was used in the laboratory. In addition to the reacted samples, REF materials were also analyzed or data were taken from former studies (e.g. Kaufhold et al., 2013; Dohrmann et al., 2013b; Fernández et al., 2022).

CEC and EC methods

The CEC was determined using the Cu-trien$_{5xcalcite}$ method (Dohrmann and Kaufhold, 2009), which uses the Cu-trien index cation that was introduced as a CEC method by Meier and Kahr
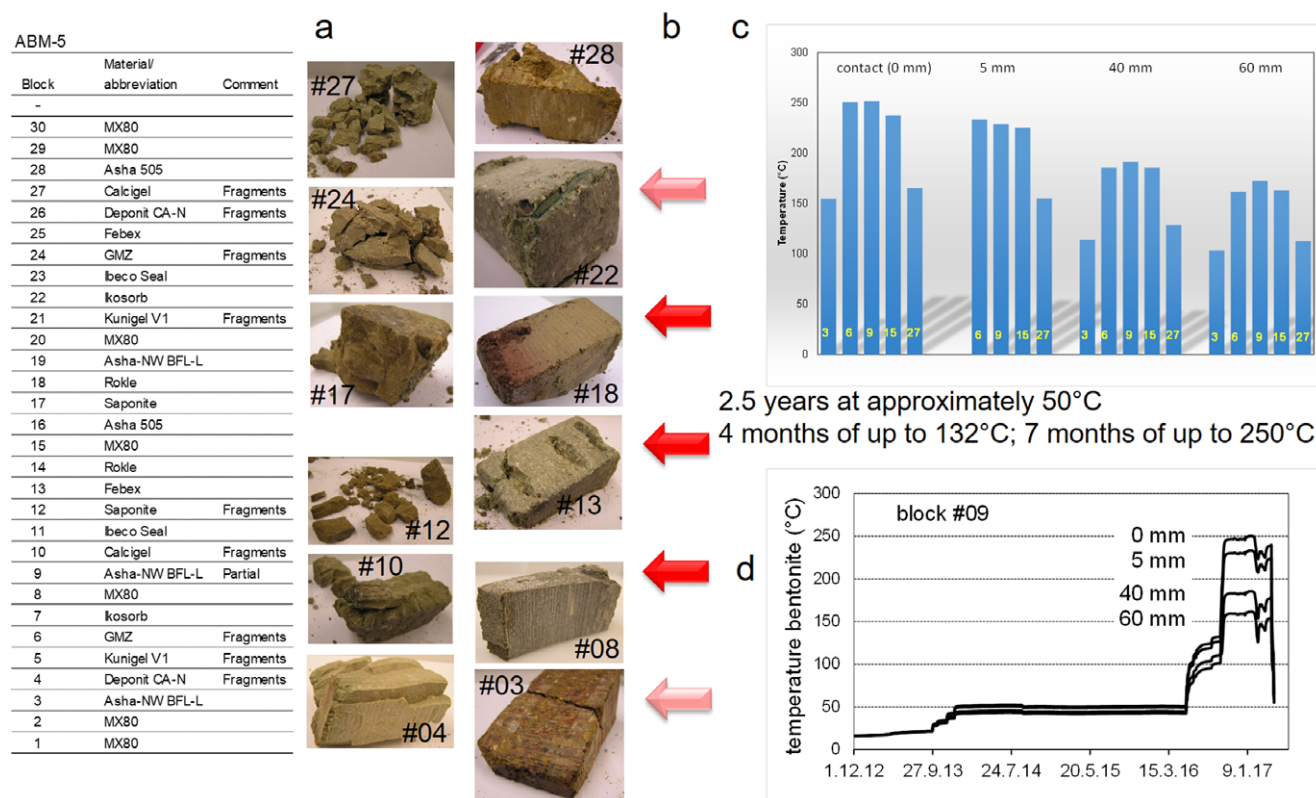
Figure 2. Influence of duration and distribution of heat impact on the ABM-5 package: (a) photographs of selected blocks of the ABM-5 experiment after dismantling; (b) schematic intensity of heat impact; (c) maximum temperatures at various depths, and (d) temperature profiles in block #09 at various distances to the heater over time.

(1999). In interlaboratory round robin tests, the Cu-trien index cation provided precise and plausible CEC and EC$_{population}$ values even for calcareous bentonites (Dohrmann et al., 2012a; Dohrmann et al., 2012b) and particularly for the exchangeable Ca^{2+} values if the Cu-trien$_{5xcalcite}$ variant of the method was used. The Cu-trien$_{5xcalcite}$ solution suppresses calcite dissolution during the exchange reaction (Dohrmann and Kaufhold, 2009) similarly to the first method based on Ag-thiourea (AgTU$_{calcite}$) using this technique of pre-equilibration of the index cation solution with fine-grained calcite and subtraction of this background Ca^{2+} concentration for calculation of exchangeable Ca^{2+} values (Dohrmann, 2006a). The Cu-trien$_{5xcalcite}$ solution was prepared by mixing 2000 mL of 0.01 M Cu-trien solution with a controlled Cu:trien ratio (cf. Stanjek and Künkel, 2016) and with 2 g of fine-grained calcite added to saturate the solution with dissolved calcite as described by Dohrmann and Kaufhold (2009). Two different sample masses were used (80 mg and 120 mg) and 10.0 mL of Cu-trien$_{5xcalcite}$ exchange solution was added to each sample in an 85 mL centrifuge tube. In contrast to Meier and Kahr (1999), no deionized water was added. For samples taken directly from the contact, only 80 mg was used and only for seven selected samples duplicates were run because of the small amounts of sample masses available. The slurry was allowed to equilibrate for 2 h in an end-over-end shaker. After Cu-trien$_{5xcalcite}$ saturation, the solutions were centrifuged to sediment the bentonite particles and separate the supernatant solutions. Solutions were diluted, acidified, and analyzed using inductively coupled plasma (ICP) spectrometry (Thermo Scientific ICAP 6300 DUO ICP-OES; Thermo Fisher Scientific, Waltham, MA, USA) to measure the ECs and Cu which allowed calculation of the CEC values. For ICP-OES analysis, the following techniques were used: argon radial plasma, nebulisers (cross-flow and

modified Lichte), no auxiliary gas flow, gain value for plasma (1.400 W), and calibration every seventh measurement. The Cu-trien complex concentration was also analyzed using VIS spectroscopy (Jenway 6200, Cole-Parmer, Staffordshire, UK) to cross-check the ICP-Cu concentration. Each CEC value was calculated by averaging four single CEC values (two from ICP analysis and two from VIS spectroscopy). Each EC value was calculated by averaging only two single EC values measured using ICP to give values in meq 100 g^{-1}. The error (± 3 sigma) of the values determined using the Cu-trien$_{5xcalcite}$ method for bentonites (Dohrmann and Kaufhold, 2009) was different for each of the exchangeable cations and the CEC.

The scattering of exchangeable cation values (± 3 sigma) was lowest for K$^+$ (± 0.3 meq 100 g^{-1}), followed by Mg^{2+} (± 0.8 meq 100 g^{-1}), Ca^{2+} (± 0.8 meq 100 g^{-1}), Na$^+$ (± 1.9 meq 100 g^{-1}), and the CEC (± 3.1 meq 100 g^{-1}). No sample had significant exchangeable Fe (all <0.1 meq 100 g^{-1} Fe^{3+}) and ECs were measured in meq 100 g^{-1}. The ECs of the different materials were also calculated as a percentage of the measured CEC value to make the EC values comparable on a %/CEC basis. If the sum of exchangeable cations exceeded 100%, the presence of typical soluble phases other than calcite, such as gypsum or halite, was indicated. The Cu-trien$_{5xcalcite}$ approach does not prevent dissolution of gypsum or halite (Dohrmann and Kaufhold, 2010). The parameter 'sum-CEC' indicates soluble minerals, such as Ca-sulfates or halite, if the value is positive, but it may also indicate salts from evaporated pore water (cf. Dohrmann et al., 2012b). In the present study, the expression 'horizontal variation' was used for EC and CEC values at radial distances between 2 and 8 cm from the heater because this part was representative of the bulk of the blocks. The 0.1 cm sample on the other hand, was important in understanding

Table 2. The blocks and sampling distances from heaters in ABM-5 used to calculate the EC (Na^+, Mg^{2+}, or Ca^{2+}) and CEC values.

Horizontal profile, individual block, 0.1 cm	$EC_{(ind.\ 0.1\ cm)}$	$CEC_{(ind.\ 0.1\ cm)}$
Horizontal profile, individual block, from 1–8 cm	$EC_{(ind.\ 1–8\ cm)}$	$CEC_{(ind.\ 1–8\ cm)}$
Average value of individual block, from 1–8 cm	$EC_{(av.\ 1–8\ cm)}$	$CEC_{(av.\ 1–8\ cm)}$
Average value of blocks 1–30, at 0.1 cm	$EC_{(av.\ blocks\ 1–30,\ 0.1\ cm)}$	$CEC_{(av.\ blocks\ 1–30,\ 0.1\ cm)}$
Average value of blocks 1–30, at 1 cm	$EC_{(av.\ blocks\ 1–30,\ 1\ cm)}$	$CEC_{(av.\ blocks\ 1–30,\ 1\ cm)}$
Average value of blocks 1–30, at 5 cm	$EC_{(av.\ blocks\ 1–30,\ 5\ cm)}$	$CEC_{(av.\ blocks\ 1–30,\ 5\ cm)}$
Average value of blocks 1–30, at 8 cm	$EC_{(av.\ blocks\ 1–30,\ 8\ cm)}$	$CEC_{(av.\ blocks\ 1–30,\ 8\ cm)}$
Average value of blocks 1–30, from 1–8 cm	$EC_{(av.\ blocks\ 1–30,\ 1–8\ cm)}$	$CEC_{(av.\ blocks\ 1–30,\ 1–8\ cm)}$
Average value of blocks 1–10, from 1–8 cm	$EC_{(av.\ lower)}$	$CEC_{(av.\ lower)}$
Average value of blocks 11–20 from 1–8 cm	$EC_{(av.\ middle)}$	$CEC_{(av.\ middle)}$
Average value of blocks 21–30, from 1–8 cm	$EC_{(av.\ upper)}$	$CEC_{(av.\ upper)}$

processes at the bentonite/heater interface; however, the contribution of this thin layer to the bulk composition was small. All of the following EC and CEC values refer to samples from different parts of individual blocks or the average values from different blocks (Table 2).

Results

Horizontal variation of the CECs and the ECs within individual blocks

As expected from ABM-1 (Kumpulainen and Kiviranta, 2011; Svensson et al., 2011; Dohrmann et al., 2013b) and ABM-2 (Kumpulainen et al., 2016; Dohrmann and Kaufhold 2017; Svensson et al., 2023), all blocks in the ABM-5 experiment showed significant differences in CEC and EC values of the blocks at various distances from the heater compared with the starting REF material.

To evaluate horizontal variations in CEC and $EC_{population}$ within individual blocks ($CEC_{(individual\ 1–8\ cm)}$, $EC_{population(individual\ 1–8\ cm)}$), six blocks from various depths in ABM-5 were selected to examine the typical variations: three new materials – GMZ (#24), 'Saponite' (#17), and Asha NW BFL-L (#19), plus Ibeco Seal (#23), MX80 (#8), and Ikosorb (#7), the latter three being selected randomly. The full dataset of all blocks is available in Tables S1 and S2 in Supplementary material.

Na^+ $EC_{(individual\ 1–8\ cm)}$ values were either larger in the outer part (GMZ #24, Asha NW BFL-L #19, MX80 #8, Ikosorb #7) of the blocks towards the cold-rock side, or more or less unchanged ('Saponite' #17) (Fig. 3). Rarely, Na^+ $EC_{(individual\ 1–8\ cm)}$ values were larger in the inner parts the blocks towards the heater (Ibeco Seal #23), with the same material showing the opposite trend at block position #11. In all blocks with a complete set of samples, Na^+ $EC_{(individual\ 1–8\ cm)}$ values were different from REF composition, and differences were significantly larger than analytical error.

For exchangeable $Mg^{2+}_{(individual\ 1–8\ cm)}$ values, two trends were observed in terms of horizontal variation: little or no variation (compare Ibeco Seal #23, Asha NW BFL-L #19, 'Saponite' #17; Fig. 3) or a decrease toward the cold-rock side (cf. GMZ #24, MX80 #8, Ikosorb #7; Fig. 3). In most blocks with a complete set of samples, Mg^{2+} $EC_{(individual\ 1–8\ cm)}$ values were different from REF composition, mostly lower. Only in some MX80 bentonites at the far end of the package (block positions #1, #2, #29 and in the center #20) were exchangeable $Mg^{2+}_{(individual\ 1–8\ cm)}$ values unchanged or increased slightly with differences larger than analytical error with respect to REF composition.

The situation was very different for exchangeable $Ca^{2+}_{(individual\ 1–8\ cm)}$ values, with four typical trends observed in terms of horizontal variation: increase towards the cold-rock side (GMZ #24, Ibeco Seal #23, Asha NW BFL-L #19, 'Saponite' #17; Fig. 3); decrease in the same direction (MX80 #8, Ikosorb #7; Fig. 3); little or negligible horizontal variation in nine other blocks not shown in Fig. 3; or changes with alternating sign in the horizontal direction. In all blocks with a complete set of samples, Ca^{2+} $EC_{(individual\ 2–8\ cm)}$ values differed from the REF composition, and differences were significantly larger than analytical error.

The exchangeable $K^+_{(individual\ 1–8\ cm)}$ values were usually too small and close to the detection limit to clearly identify any changes.

$CEC_{(individual\ 1–8\ cm)}$ values were either larger in the outer parts (Ibeco Seal #23, Asha NW BFL-L #19, 'Saponite' #17; Fig. 3) of the blocks toward the cold-rock side, or more or less unchanged (GMZ #24, MX80 #8 Ikosorb #7; Fig. 3). In contrast to $EC_{population\ (individual\ 1–8\ cm)}$ values, $CEC_{(individual\ 1–8\ cm)}$ values were relatively similar to the REF composition, and differences were mostly (in 61 cases) less than analytical CEC error (±3.1 meq 100 g^{-1}, 3 sigma). In 11 cases, differences were larger than analytical CEC error. In three cases, differences were between two and three times ±3.1 meq 100 g^{-1}: MX80 #30 and Febex #13 with a CEC decrease, and Ibeco Seal #11 with a CEC increase.

Chloride$_{(individual\ 1–8\ cm)}$ concentration in most blocks showed no horizontal variation (compare 'Saponite' #17, Ikosorb #7) (Fig. 3); however, in a few blocks the chloride$_{(individual\ 1–8\ cm)}$ concentration varied with either a maximum at 5 cm (compare MX80 #8; Fig. 3) or a minimum. In five cases an increase and in two cases a decrease in chloride$_{(individual\ 1–8\ cm)}$ concentration towards the rock side was observed. In most blocks with a complete set of samples, chloride$_{(individual\ 1–8\ cm)}$ values were larger compared with the REF composition (all blocks in Fig. 3), with a few exceptions such as Asha 505 (#28, #16) and Ikosorb (#22), (compare also Table S2). Note that the chloride concentrations were not measured by aqueous extracts or CEC extract solutions but determined by whole-rock chemical analysis (INAA; Table S1) taken from Kaufhold et al. (2021).

Variation of CECs and ECs on a larger horizontal and vertical scale

To obtain an overview of large-scale horizontal and also vertical exchange processes in ABM-5 over many different bentonite blocks, average values of CECs and ECs were calculated for blocks 1–30. The whole package was further subdivided into three parts (lower, middle, and upper). Total gains and losses in ECs and CECs were calculated as percentages with respect to the REF values for:

(1) All blocks at each distance from the heater (CEC/ $EC_{(av.\ blocks\ 1–30,\ 0.1\ cm,\ 1\ cm,\ 5\ cm,\ 8\ cm)}$) (Fig. 4a) representing vertical average values at these positions relative to the heater;
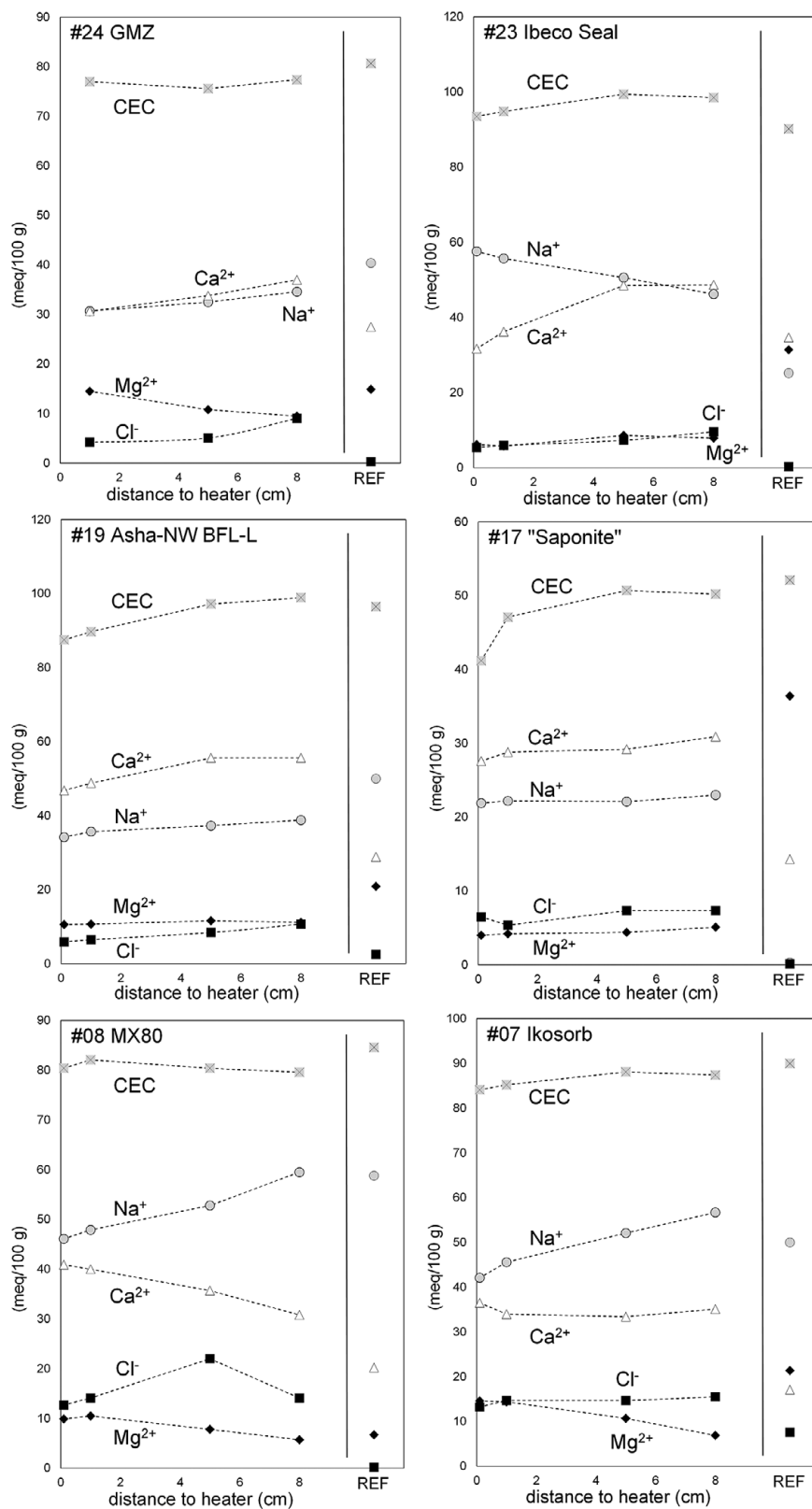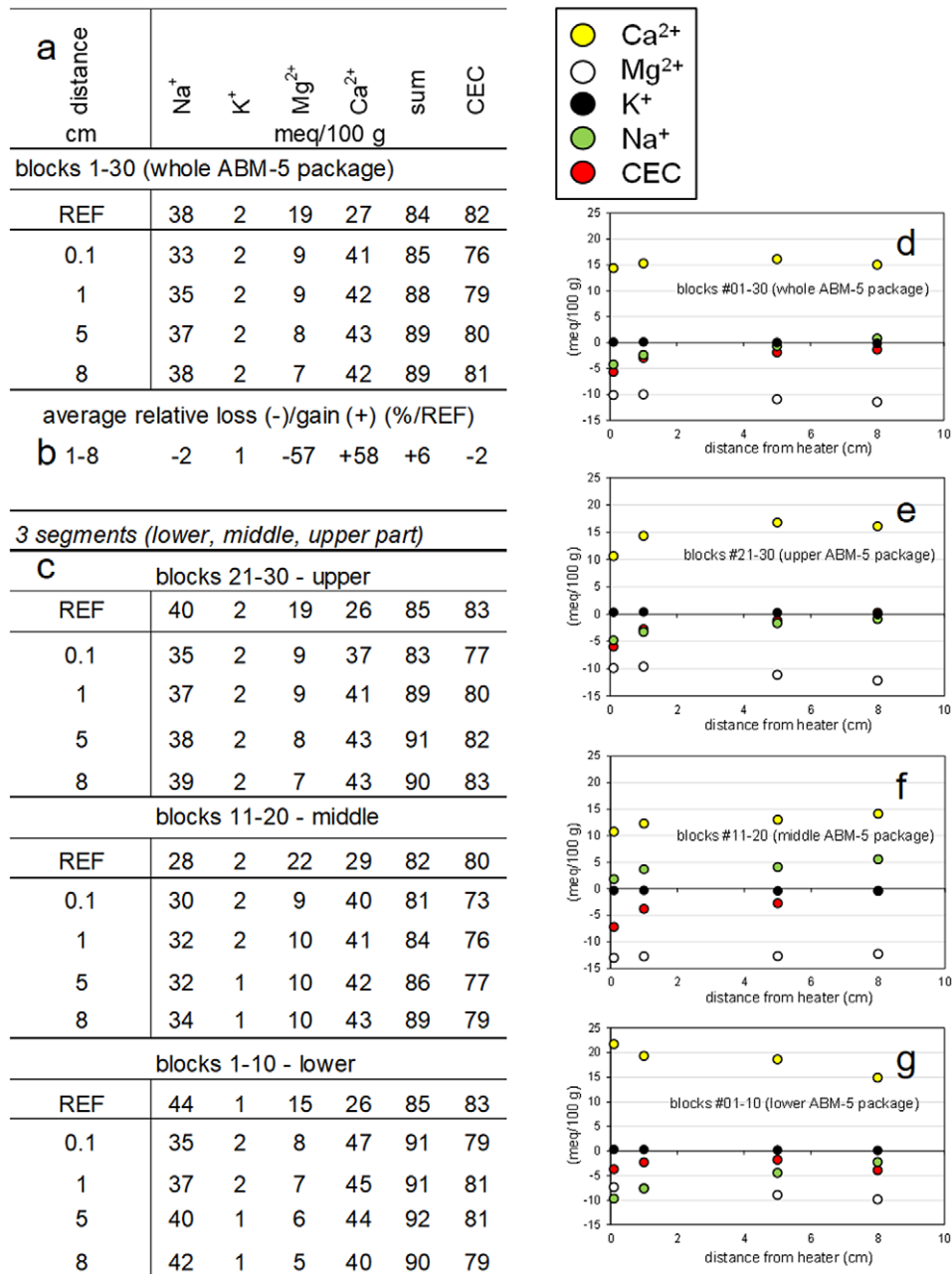
Figure 3. Examples of the different horizontal EC and CEC distributions of the various blocks. The block numbers are indicated in the label boxes at the top of each graph before the sample name.

a — distance cm | Na^+ | K^+ | Mg^{2+} | Ca^{2+} | sum | CEC (meq/100 g)

distance cm	Na^+	K^+	Mg^{2+}	Ca^{2+}	sum	CEC
blocks 1-30 (whole ABM-5 package)						
REF	38	2	19	27	84	82
0.1	33	2	9	41	85	76
1	35	2	9	42	88	79
5	37	2	8	43	89	80
8	38	2	7	42	89	81
b — average relative loss (-)/gain (+) (%/REF)						
1-8	-2	1	-57	+58	+6	-2
c — *3 segments (lower, middle, upper part)*						
blocks 21-30 - upper						
REF	40	2	19	26	85	83
0.1	35	2	9	37	83	77
1	37	2	9	41	89	80
5	38	2	8	43	91	82
8	39	2	7	43	90	83
blocks 11-20 - middle						
REF	28	2	22	29	82	80
0.1	30	2	9	40	81	73
1	32	2	10	41	84	76
5	32	1	10	42	86	77
8	34	1	10	43	89	79
blocks 1-10 - lower						
REF	44	1	15	26	85	83
0.1	35	2	8	47	91	79
1	37	2	7	45	91	81
5	40	1	6	44	92	81
8	42	1	5	40	90	79

Figure 4. Average values: (a) (0.1–8 cm) over the whole ABM-5 package with the individual Cu-trien$_{5xcalcite}$ values (meq 100 g^{-1}) for ECs, sum of ECs, and CECs of all the ABM-5 samples including values of reference (REF) samples taken from Table 1; (b) total relative (%) differences of averages of all blocks from 1 to 8 cm (CEC/EC$_{(av.\ blocks\ 1–30,\ 1–8\ cm)}$) with respect to REF values; (c) average values at these distances of three segments (lower, middle, and upper parts) at the various depths sampled; (d) graphical representation of changes in the average values with respect to REF values (all blocks) at the various depths sampled; (e, f, g) graphical representation of changes in the average values with respect to REF values of three parts (lower, middle, and upper) at the various depths sampled. Note that blocks #3, #4, #6, #9, #12, #24, and #27 were partly disintegrated and could not be analyzed using the expected scheme as indicated in Fig. 1.

(1) Averaged over the entire package, vertical EC$_{(av.\ blocks\ 1–30,\ 0.1\ cm,\ 1\ cm,\ 5\ cm,\ 8\ cm)}$ gradients at each distance were detected for exchangeable Na$^+$: decrease from 38 to 33% from the rock side to the hot part, with 38% being the starting composition of REF samples. Exchangeable Mg^{2+} on the other hand decreased by half with respect to the REF composition and showed a further decrease from 9 to 7% in the opposite direction from the hot to cold side (Fig. 4a). Vertically, exchangeable Ca^{2+} values increased generally with respect to the REF composition and showed no gradients at various distances from the rock to the heater. CECs on the other hand showed gradients but in opposite directions, with smaller

(2) Total relative (%) differences of these vertical averages from 1 to 8 cm (CEC/EC$_{(av.\ blocks\ 1–30,\ 1–8\ cm)}$) with respect to REF values (Fig. 4b);
(3) Horizontal distances of 0.1, 1, 5, and 8 cm for units that consisted of segments of ~10 blocks (upper (21–30), middle (11–20), and lower part (1–10)), CEC/EC$_{(av.\ upper,\ middle,\ lower)}$ (Fig. 4c).

Note that the average EC and CEC values depended on both the interaction with saline Äspö groundwater at elevated temperatures and the different EC$_{population}$ of the starting materials packed on each other. The EC$_{population}$ changed during the experiment as expected from former ABM experiments.

CEC values towards the hot part (decrease from 81 to 76 meq 100 g^{-1}). At distances of between 1 and 8 cm, the CEC decrease was scarcely distinguishable from analytical error. All of the observed differences were relatively small in relation to the analytical errors of the method.

(2) In total, the exchangeable Na$^+$$_{(av.\ blocks\ 1-30,\ 1-8\ cm)}$ and Mg^{2+}$_{(av.\ blocks\ 1-30,\ 1-8\ cm)}$ values decreased in ABM-5 by 2% and 57%, respectively, relative to REF materials, whereas the exchangeable Ca^{2+}$_{(av.\ blocks\ 1-30,\ 1-8\ cm)}$ values increased by 58%. Average CECs decreased by 2% and sum-CEC values increased by 6%. Note that these are relative changes, not absolute changes (Table 3).

(3) Considering absolute average vertical differences in various segments (lower-upper part) allows us to evaluate EC modifications on this intermediate scale. Graphical representation of changes in the differences of average values in relation to REF values in the lower, middle, and upper segments shows clearly various gains and losses in terms of EC and CEC values (Fig. 4d–g). Exchangeable Na$^+$ increased absolutely in the middle part (4% exchangeable Na$^+$$_{(av.\ middle)}$), in comparison with the upper and lower parts (–3% and –6% exchangeable Na$^+$$_{(av.\ upper,\ lower)}$). The average absolute losses of Mg^{2+}$_{(av.\ upper\ and\ middle)}$ and Mg^{2+}$_{(av.\ lower)}$ were similar for the upper and middle parts of ABM-5 (11% and 13%, respectively). In the lower part, the exchangeable Mg^{2+}$_{(av.\ lower)}$ values decreased by 8% only. The same uniform modification but with different sign was observed for Ca^{2+}$_{(av.\ upper\ and\ middle)}$ with 14% and 13% increase, whereas in the segment at the bottom, Ca^{2+}$_{(av.\ lower)}$ showed a stronger increase of 19%. CECs showed the same losses of 2–4% anywhere in the three segments.

Average EC and CEC values in the entire ABM-5 package

In order to understand ion exchange processes by interactions with groundwater, the average EC and CEC values (CEC/EC$_{(av.\ 1-8\ cm)}$) in the horizontal direction of all individual blocks of the reacted ABM-5 package were calculated. Note that these values were averaged from horizontal profiles including concentration gradients at distances of 1, 5, and 8 cm from the heater. These samples, however, represent the bulk composition of the blocks and samples from direct contact with the heater were not used as these represent just a few per cent of the blocks but differ in composition markedly from other parts of the blocks. The following blocks were fractured and could not be sampled at all distances: #3, #4, #6, #9, #12, #24, #27. Average values were calculated from the available sampled parts (compare full dataset; Table S1).

On this block-wise scale, it is useful to compare the EC values as percentage values instead of meq 100 g–1 values to detect trends because EC differences can be compared directly also for materials with very different REF CECs ranging from 52 to 101 meq 100 g^{-1}. For example, a decrease of 13 meq 100 g^{-1} exchangeable Mg^{2+} in Calcigel (#27) with a REF CEC of 65 meq 100 g^{-1} and a reacted CEC of 64 meq 100 g^{-1} equals a decrease of 20% Mg^{2+}/CEC. A decrease of 18 meq 100 g^{-1} exchangeable Mg^{2+} is much more on an absolute scale; however, in Febex bentonite (#25) with a REF CEC of 101 meq 100 g^{-1} and a reacted CEC of 98 meq 100 g^{-1}, this equals 18% Mg^{2+}/CEC and means that exchangeable Mg^{2+} differences are similar on a percentage basis. Comparing 12 different bentonites at 30 different positions with four different ECs allowed an easier view of relative changes in the package. Percentage values were calculated as follows: Na$^+$ (%/CEC) = Na$^+$ (meq 100 g^{-1})/CEC (meq 100 g^{-1}) and used in Table 3 and Fig. 5. The same was done for the other EC

parameters. Note that this calculation was made for REF materials as well as for reacted samples. The CEC$_{REF}$ values were used for EC$_{REF}$ calculation. For average EC calculation of individual blocks of reacted samples, the average CEC values of the reacted samples in that block were used. Based on this calculation procedure, the sum of ECs may not fully match with the CEC both in REF materials and reacted samples. An overview of the differences in the REF materials (CEC$_{REF}$, EC$_{REF}$) (Table 3) and a comparison of ABM-5 to ABM-1 and ABM-2 were, thus, possible.

Average exchangeable Mg^{2+}$_{(av.\ 1-8\ cm)}$ values decreased in most blocks in comparison with the starting materials, whereas Na$^+$$_{(av.\ 1-8\ cm)}$ values decreased and increased in many blocks. Summing up all these differences for Na$^+$$_{(av.\ 1-8\ cm)}$ values resulted in totals at the same level as REF samples. Exchangeable Ca^{2+}$_{(av.\ 1-8\ cm)}$ values on the other hand increased significantly (Table 3). For the average EC$_{population}$ in all the analyzed blocks, the Ca^{2+}$_{(av.\ 1-8\ cm)}$ values were greatest (54%), followed by Na$^+$$_{(av.\ 1-8\ cm)}$ (46%), Mg^{2+}$_{(av.\ 1-8\ cm)}$ (10%), and K$^+$$_{(av.\ 1-8\ cm)}$ (2%).

Bar graphs indicate changes in the REF samples *versus* the reacted samples (Fig. 5). CEC or EC differences oriented to the left indicate a loss in CEC (Fig. 5a) or a loss in the respective exchangeable cation (Fig. 5b). Gains ended up in an orientation of the bars to the right (positive values), which was always the case for the difference sum–CEC (Fig. 5c). The most pronounced EC changes were found for the bentonite block with trioctahedral smectites ('Saponite' #12, #17), which were initially rich in exchangeable Mg^{2+}. The smallest changes were observed for GMZ bentonite (#6, #24) with a starting composition relatively close to the average composition of all reacted samples.

On an individual block level, only Na$^+$-rich bentonites with ~50% Na$^+$$_{(av.\ 1-8\ cm)}$ reduced their exchangeable Na$^+$ content (Fig. 6a), but not always. In the lower section, some blocks with ≥50% Na$^+$$_{(av.\ 1-8\ cm)}$ (blocks #9, #7, #6) ended with an increase in exchangeable Na$^+$. The largest loss of 44% Na$^+$$_{(av.\ 1-8\ cm)}$ was observed for MX80 (#2). Bentonites starting with <40% initial exchangeable Na$^+$ showed a clear increase of up to 53% with the largest final percentage value for Calcigel (#10).

Six of seven reacted MX80 bentonite blocks starting with 8% Mg/CEC (REF) showed a small increase of mostly 1 or 2% Mg^{2+}/CEC, with exceptions of 4% and a small decrease of 1% (Table 3). The other low Mg-bentonite Kunigel V1 (2% REF concentration) was also enriched in exchangeable Mg^{2+} (1% and 3%); however, all other blocks lost exchangeable Mg^{2+} (Table 3). Mg^{2+}-rich bentonites ('Saponite') lost nearly all exchangeable Mg^{2+}$_{(av.\ 1-8\ cm)}$; significant Mg^{2+}$_{(av.\ 1-8\ cm)}$ loss was observed whenever bentonites started with >10% initial exchangeable Mg^{2+}/CEC (Fig. 6b). According to the losses described for exchangeable Na$^+$ and Mg^{2+}, only a few Ca^{2+}-rich bentonites with initial REF concentrations of >70% lost exchangeable Ca^{2+}$_{(av.\ 1-8\ cm)}$ (Fig. 6c) whereas most bentonites took up lots of exchangeable Ca^{2+}$_{(av.\ 1-8\ cm)}$.

In total, ECs increased by 10% compared with REF values (+1% Na$^+$/CEC, –12% Mg^{2+}/CEC, +21% Ca^{2+}/CEC) with, on average, a significant excess of sum of extracted cations in the range of 10% of the CEC (average) resulting in a sum–CEC$_{(av.\ 1-8\ cm)}$ = 7 meq 100 g^{-1} (Table 3). This excess means that the amount of soluble salts providing cations calculated as EC values that were not present in the interlayer increased.

Differences in the CEC values between the REF materials and the bulk average values (CEC$_{(av.\ 1-8\ cm)}$) were typically lower than the reproducibility (±3.1 meq 100 g^{-1}, ±3 sigma) of the applied method. Only a few samples showed larger deviations of +7 and +8 meq 100 g^{-1} (Ibeco Seal #23, Calcigel #10).
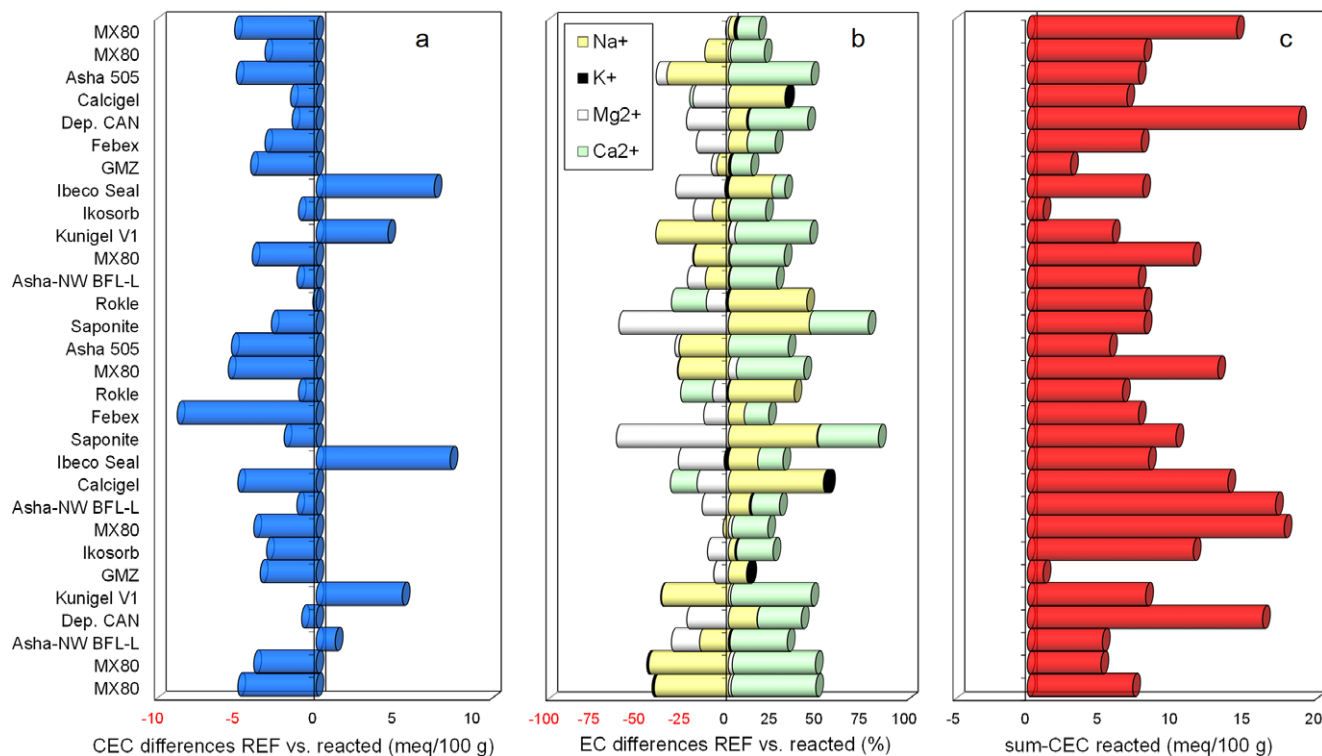
Table 3. The 1–8 cm sample average EC (%), CEC, and 'sum–CEC' values (both meq 100 g^{-1}) of the ABM-5 samples measured using the Cu-trien$_{5xcalcite}$ method.

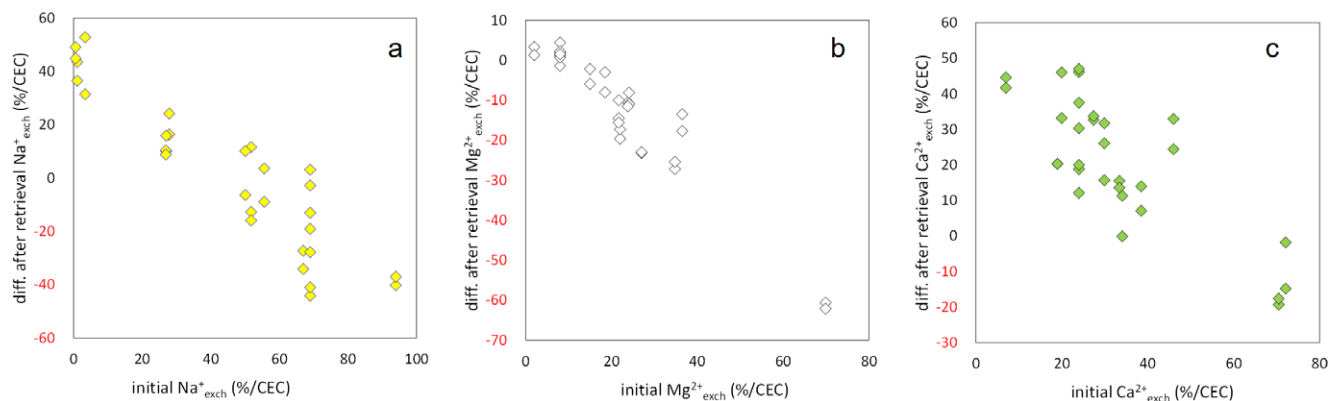| Block	Material/abbreviation	Na$^+$	K$^+$	Mg^{2+}	Ca^{2+}	CEC	sum-CEC	Na$^+$	K$^+$	Mg^{2+}	Ca^{2+}	CEC	sum-CEC	Na$^+$	K$^+$	Mg^{2+}	Ca^{2+}	CEC	sum-CEC
		reference material (%)				(meq/100 g)		retrieved samples 1–8 cm (averages) (%)				(meq/100 g)		differences (neg=lost) (% absolute)				(meq/100 g)	
30	MX80	69	2	8	24	85	3	72	4	7	36	80	15	3	2	−1	12	−5	12
29	MX80	69	2	8	24	85	3	56	2	9	43	81	8	−13	0	1	19	−3	6
28	ASha 505	67	1	15	20	91	3	33	1	9	66	86	8	−34	0	−6	46	−5	5
27	Calcigel	3	2	22	72	65	0	35	3	2	70	64	7	31	1	−20	−2	−2	7
26	Dep. CAN	27	2	27	46	84	2	37	3	4	79	82	19	10	1	−23	33	−2	17
25	Febex	27	3	37	33	101	0	37	3	19	49	98	8	10	0	−18	16	−3	8
24	GMZ	50	1	19	34	81	3	44	2	16	45	77	3	−6	1	−3	11	−4	0
23	Ibeco Seal	28	5	35	39	90	5	52	3	8	46	98	8	24	−2	−27	7	7	3
22	Ikosorb	56	2	24	19	90	0	47	2	13	39	89	1	−9	0	−11	20	−1	1
21	Kunigel V1	94	1	2	7	61	2	54	1	5	49	66	6	−40	0	3	42	5	4
20	MX80	69	2	8	24	85	3	50	1	9	54	81	12	−19	−1	1	30	−4	9
19	Asha-NW BFL-L	52	1	22	30	97	4	39	1	12	56	95	8	−13	1	−10	26	−1	4
18	Rokle	1	3	24	71	74	−1	45	2	13	51	74	8	44	−1	−11	−19	−0	9
17	Saponite	1	2	70	27	52	0	46	2	9	60	49	8	45	−0	−61	33	−3	8
16	Asha 505	67	1	15	20	91	3	40	1	13	53	86	6	−27	−0	−2	33	−5	3
15	MX80	69	2	8	24	85	3	41	2	12	62	79	13	−28	−0	4	38	−6	11
14	Rokle	1	3	24	71	74	−1	38	3	16	53	73	7	37	−1	−8	−18	−1	7
13	Febex	27	3	37	33	101	0	36	3	23	47	93	8	9	−0	−14	14	−9	8
12	Saponite	1	2	70	27	52	0	50	2	8	61	50	10	49	1	−62	34	−2	11
11	Ibeco Seal	28	5	35	39	90	5	44	3	9	53	99	8	16	−2	−25	14	8	3
10	Calcigel	3	2	22	72	65	0	56	5	5	57	60	14	53	2	−17	−15	−5	14
9	Asha-NW-BFL-L	52	1	22	30	97	4	63	2	7	46	95	17	12	1	−15	16	−1	13
8	MX80	69	2	8	24	85	3	66	2	10	44	81	18	−3	−0	2	20	−4	15
7	Ikosorb	56	2	24	19	90	0	59	3	12	39	87	12	4	1	−12	20	−3	12
6	GMZ	50	1	19	34	81	3	60	2	11	34	77	1	10	1	−8	−0	−4	−2
5	Kunigel V1	94	1	2	7	61	2	57	1	3	52	66	8	−37	−1	1	45	5	6
4	Dep. CAN	27	2	27	46	84	2	43	2	4	70	83	16	16	0	−23	24	−1	15
3	Asha-NW BF-L	52	1	22	30	97	4	36	2	6	62	98	5	−16	1	−16	32	1	1
2	MX80	69	2	8	24	85	3	25	1	10	70	81	5	−44	−1	2	46	−4	3
1	MX80	69	2	8	24	85	3	28	1	10	71	80	7	−41	−1	2	47	−5	5
	averages #1–30	45	2	22	33	82	2	46	2	10	54	80	9	1	0	−12	21	−2	7

Exchangeable cation distribution and Cl$^-$ uptake over the entire ABM-5 package

During the experiment, the blocks took up groundwater while being heated. In ABM-1, after retrieval of the package, no horizontal gradients were observed. That was very different from the case in ABM-5. Regarding horizontal EC gradients of reacted ABM-5 samples, the question arose as to why no equilibrium was reached or, if equilibrium was reached in-between during the heater experiment, why it was changed again. Two parameters were used for this analysis: Na$^+$/Mg^{2+} ratios and chloride concentration.

Exchangeable Na$^+$ and Mg^{2+} values were slightly inflated by uptake of groundwater. The sum–CEC differences were, on average, 7 meq 100 g^{-1} larger compared with REF materials and much of that can be attributed to measured exchangeable Ca^{2+} values. Therefore, the Na$^+$/Mg^{2+} ratio and the gains and losses in Na$^+$$_{(av. 1–8 cm)}$ and Mg^{2+}$_{(av. 1–8 cm)}$ values (Na$^+$/Mg^{2+} ratio $_{(av. 1–8 cm)}$) were investigated in more detail (Fig. 7). After installation and before the heating of ABM-5, the Na$^+$/Mg^{2+} ratios of the REF samples varied from <0.1 (Rokle) to 47 (Kunigel V1). Nine bentonites had Na$^+$/Mg^{2+} ratios $_{(av. 1–8 cm)}$ >5 (two blocks of Kunigel V1 and all seven blocks of MX80). These blocks were

Figure 5. Bar graphs to indicate the changes in the REF samples *versus* the reacted samples: (a) CEC, (b) EC, and (c) the sum of the ECs–CEC (sum–CEC) values at the end of the test for the 1–8 cm samples (averages) for all blocks of ABM-5 (Table 3).
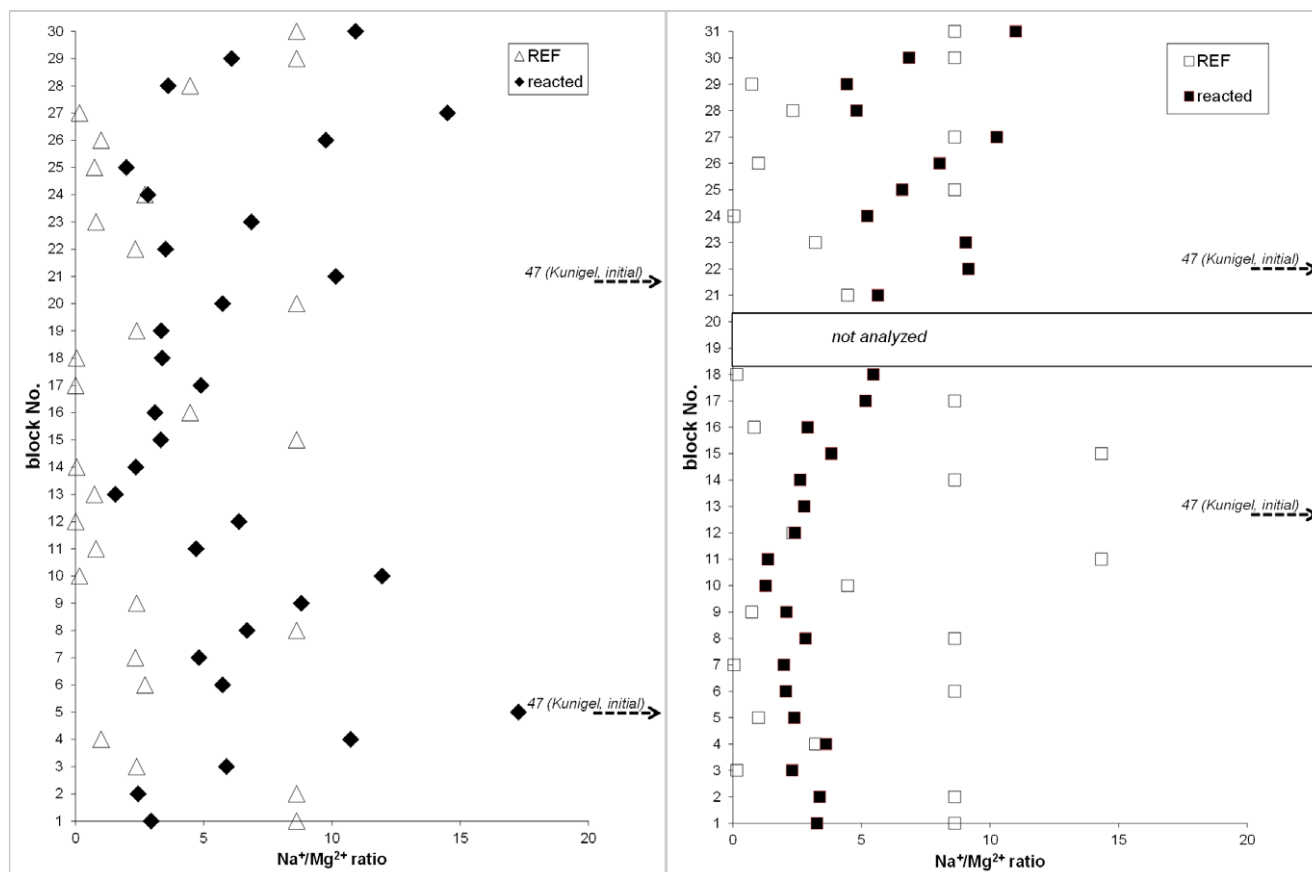

Figure 6. Differences in average EC values (%/CEC) with respect to REF concentrations: (a) $Na^+_{(av.\ 1-8\ cm)}$; (b) $Mg^{2+}_{(av.\ 1-8\ cm)}$; (c) $Ca^+_{(av.\ 1-8\ cm)}$.

distributed evenly from the bottom to the top of ABM-2 with MX80 as the two top and two bottom blocks (Fig. 7). After retrieval, however, a distinction could be made between the Na^+/Mg^{2+} ratios of the central part compared with the upper and lower parts of the package. In the central part between position #13 and #19 the ratio was always <5 and some blocks had Na^+/Mg^{2+} ratios $_{(av.\ 1-8\ cm)}$ >5 at lower and upper positions: Ibeco Seal, Asha-NW BFL-L, and 'Saponite'. This indicated that locally different conditions affected the cation equilibration. Looking at all 30 blocks, 11 blocks had significant changes in Na^+/Mg^{2+} ratios $_{(av.\ 1-8\ cm)}$ of >5 indicating a strong distribution of the exchangeable Na^+ and Mg^{2+} values over the entire ABM-5 package.

Chloride access to smectitic interlayer positions in highly compressed bentonite blocks is limited (e.g. Tournassat and Appelo, 2011). Accordingly, this anion should have a low ability to be

distributed over the entire package as observed for cation exchange. The difference, however, was observed in ABM-5 (Fig. 8). During the uptake of groundwater obviously not only cation exchange but also uptake of excess electrolyte including anions took place. In three cases, a block lost chloride compared with REF concentration (Asha 505, #28, #16; Ikosorb, #22) and in all other blocks, chloride increased with the result that chloride concentrations have been balanced between bentonite blocks. In general much more chloride was taken up, increasing the parameter sum–CEC$_{(av.\ 1-8\ cm)}$ to, on average, 7 meq 100 g^{-1} (Table 3; Fig. 5c).

At first view this trend can be followed by the good correlation of chloride concentration with the parameter sum–CEC $_{(av.\ 1-8\ cm)}$ (Fig. 8a). Dividing the blocks by position above and below the center indicates that more chloride entered the lower half of the package. Note that data were compared from two completely

Figure 7. Plot of block number *versus* Na$^+$/Mg^{2+} ratios for exchangeable Na$^+$$_{(av.\ 1-8\ cm)}$ and Mg^{2+}$_{(av.\ 1-8\ cm)}$ (filled symbols) in ABM-5 of reacted samples in comparison with the Na$^+$/Mg^{2+} ratios for the REF samples (open symbols).

different analytical methods: aqueous extraction data (ABM-1/-2 samples only; Dohrmann et al., 2013b) and INAA analysis (Kaufhold et al., 2021). This correlation of both techniques is good and can be followed by tabulated data of REF samples in the inset (Fig. 8b).

Chloride content in the pore water of all REF blocks (Fig. 8c) in the initial state (blue) and after retrieval of the package (red) (Fig. 8d) supports the observation that chloride was taken up more strongly in the lower half (Fig. 8a).

The parameter sum–CEC$_{(av.\ 1-8\ cm)}$ had strong positive values both in the upper and in the lower half of the ABM-5 package; however, only in the lower half did this correlate with the uptake of Cl$^-$. Another anion may explain this discrepancy: sulfate Cl$^-$ concentrations of reacted-REF materials were mostly positive, thus explaining differences in sum–CEC of reacted-REF materials (all related to %/CEC$_{REF}$) in SO$_4$$^{2-}$-free REF materials (Fig. 8e), whereas in REF materials with SO$_4$$^{2-}$-rich minerals (gypsum) the correlation was poor (Fig. 8f). The best correlation of 'sum–CEC' *versus* Cl$^-$ for blocks without sulfate-bearing samples was found in the vertical direction at '5 cm' ($n=15$, $R^2=0.66$) compared with the average Cl concentration ($n=30$, $R^2=0.59$).

Discussion

The aims of the present study are discussed by comparing data from the three ABM packages which have been terminated and sampled already: ABM-1, -2, and -5 (Table 4).

Horizontal variation of the CECs and the ECs within individual blocks

In ABM-1, no significant horizontal gradients in the EC$_{population}$ were detected in the blocks analyzed (Kumpulainen and Kiviranta, 2011 (studying 4 blocks), Svensson et al., 2011 (studying 11 blocks), and Dohrmann et al., 2013b (studying 21 blocks)).

In ABM-2, horizontal gradients of CEC $_{(individual\ 1-8\ cm)}$ and EC $_{(individual\ 1-8\ cm)}$ values in single blocks were detected, mainly in the upper part (Kumpulainen et al., 2016 (studying 3 blocks), Dohrmann and Kaufhold, 2017 (studying 29 blocks)); however, an examination of the horizontal gradients in these single blocks failed to help understand the trends.

In the present study, pronounced horizontal gradients of EC$_{population}$ in single blocks were observed (Fig. 3; Table S2) for all measured parameters including also total CEC values (CEC/EC $_{(individual\ 1-8\ cm)}$) in ABM-5. Horizontal variations of CEC and EC$_{population}$ values within individual blocks (CEC $_{(individual\ 1-8\ cm)}$, EC$_{population\ (individual\ 1-8\ cm)}$) of reacted ABM-5 samples were relatively large compared with ABM-1 and ABM-2.

Cation exchange processes were also studied in five of the 30 compacted ABM-5 blocks made of MX80, Rokle, Febex, Ibeco Seal, and Asha NW BFL-L (blocks #3, #11, #13, #14, #30) by Kumar et al. (2021). Those authors identified a relative decrease in exchangeable Na$^+$ cations toward the contact zone in MX-80, Asha NW BFL-L, Febex, and Rokle bentonites without commenting on exchangeable Ca^{2+} and Mg^{2+} cations. Fernández et al. (2022) reported on pore-water composition, EC, and CEC data of five blocks made of
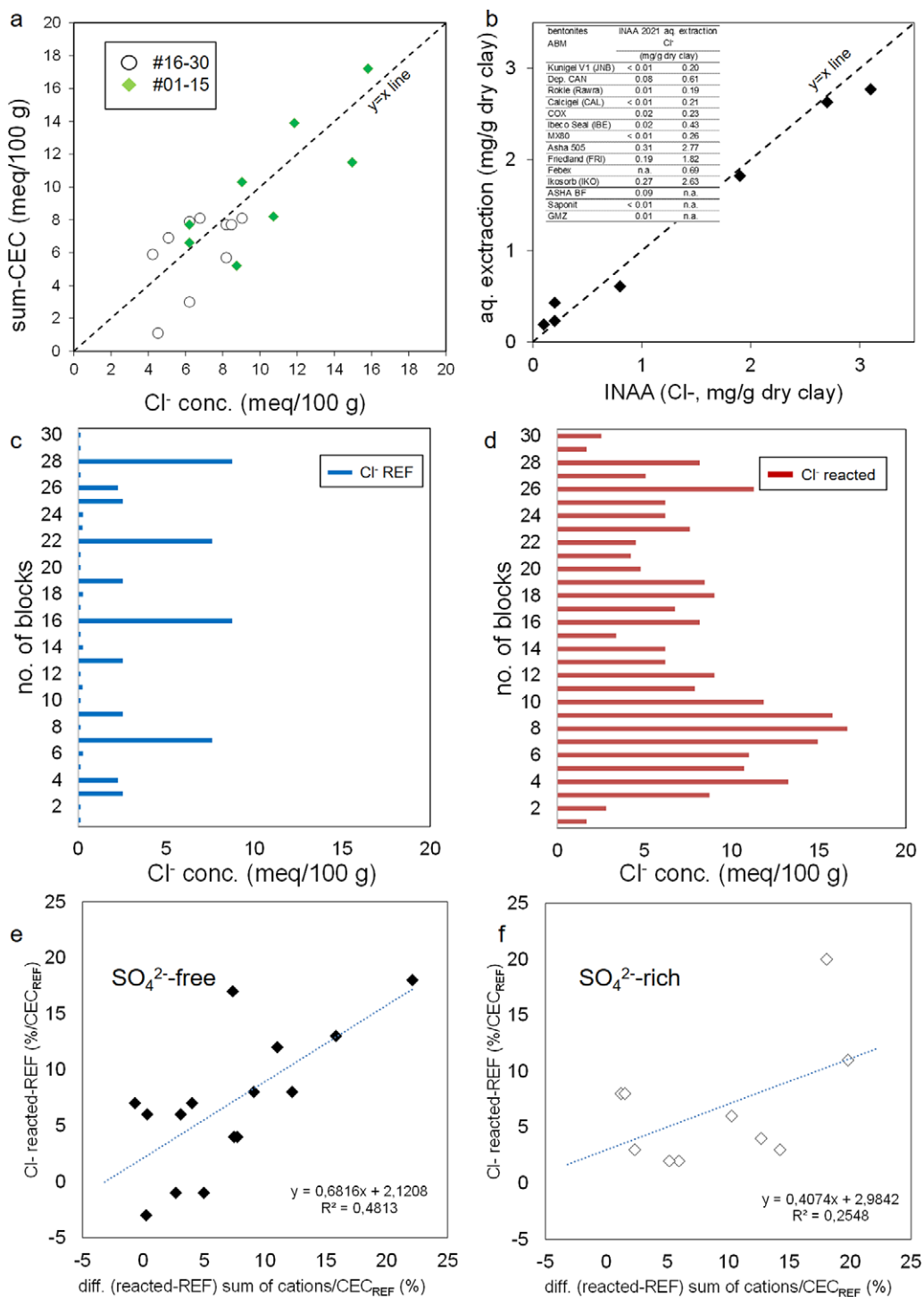
Figure 8. (a) Impact of chloride concentration on 'sum–CEC' of all blocks (without sulfate-bearing samples), #1–15 (upper part) circles, #16–30 (lower part) diamonds. (b) Comparability of aqueous extraction data (ABM-1/-2 samples only; Dohrmann et al., 2013b) with INAA analysis (Kaufhold et al., 2021). Distribution of chloride in the pore water of all blocks: (c) in the initial state (blue); and (d) after retrieval of the package (red). (e) Differences in Cl^- concentration of reacted-REF materials were mostly positive, explaining differences of sum–CEC of reacted-REF materials (all related to $\%/CEC_{REF}$) in SO_4^{2-}-free REF materials whereas in (f) REF materials with SO_4^{2-}-rich minerals (gypsum) correlation was poor. Note that Cl^- average values were calculated from 1–8 cm for all but the following blocks: #3, 1 and 5 cm; #4, 1 and 6 cm; #6, distance not specified; #9, 3 cm; #12, 8 cm; #27, 7 and 8 cm.

MX-80, Ibeco Seal, Rokle, Febex, and Asha 505 (blocks #1, #11, #14, #25, #28). Those authors described an increase in exchangeable Ca^{2+} in all bentonites other than Rokle, and a decrease in exchangeable Mg^{2+} in all bentonites but MX80, whereas exchangeable Na^+ showed both trends. Some of these trends depended on the starting

composition which varied significantly (cf. Dohrmann et al., 2013b, reporting this general process for ABM-1). Svensson et al. (2023) studied four blocks made of Calcigel, Deponit CAN, MX80, and Asha 505 (blocks #16, #20, #26, #27). That study confirmed the general trends for ECs described previously.

When discussing EC values, an excess with respect to the index cation CEC value is reported. CEC is not an absolute property; however, as a working hypothesis, the CEC value can be regarded as a kind of 100% criterion for the buffer materials studied. Under this premise, all extracted cations above the CEC value (exceeding analytical errors) may not be meaningful and have to be checked for plausibility.

The observed increase in sum–CEC values in ABM-5 points to an excess of electrolyte in these CEC experiments, sources being either soluble Ca-sulfate phases such as gypsum or anhydrite present in some REF and reacted blocks (cf. Kaufhold et al., 2017a), which increased exchangeable Ca^{2+} values or groundwater causing an excess of chloride by evaporation of groundwater (Dohrmann and Kaufhold, 2017).

On the identical sample set, Kaufhold et al. (2021) could not identify neo-formation of gypsum or anhydrite as soluble Ca-phases in reacted ABM-5 bentonites. Gypsum concentrations decreased with respect to REF materials and anhydrite was not found in any sample. To verify this absence of influence of sulfates on ABM-5 $EC_{population}$, the same quantification was used as in Dohrmann and Kaufhold (2017) who studied ABM-2 excess cations in reacted samples. Gypsum concentrations were quantified using the differences between the elemental sulfur concentrations of the reacted samples and the REF samples. Assuming that Ca-sulfate phases were dissolved completely during a CEC experiment, the inflated Ca^{2+} values were calculated and used to correct the actual exchangeable Ca^{2+} values as discussed by Dohrmann and Kaufhold (2010). In the ABM-5 package, the increase in measured exchangeable Ca^{2+} values showed a poor correlation with the 'calculated inflated exchangeable Ca^{2+}' values based on gypsum dissolution. One sample was close to the $y = x$ line (Fig. 9) and this '1 cm sample' from the top block (MX80, #30) showed neo-formation of gypsum in SEM profiles from heater contact into the bentonite (Kaufhold et al., 2021). In total, six of 99 available data points showed calculated inflated exchangeable Ca^{2+} values of ≥5 meq $100 \ g^{-1}$. Values for exchangeable Ca^{2+} on the x-axis for ABM-5 were, on average, +18 meq $100 \ g^{-1}$ (= +21% Ca^{2+}/CEC) which is

much less than for ABM-2 (average = +48 meq $100 \ g^{-1}$, respectively, +41% Ca^{2+}/CEC; Dohrmann and Kaufhold (2017). In both ABM experiments, sulfate phases were not indicative of the overall excess plotted on the y-axis: ABM-5 (average = −2 meq $100 \ g^{-1}$) and ABM-2 (average = 0 meq $100 \ g^{-1}$). Accordingly, soluble Ca-sulfates are not the source of the general increase in exchangeable Ca^{2+} values.

### Average EC and CEC values for Na^+/Mg^{2+} ratios in the entire ABM-5 package

Cation exchange is the first reaction taking place in bentonite barriers throughout the saturation process and will end up with an equilibrium cation population. The performance of the barrier will depend on the resulting cation population and, hence, is of more interest than the initial cation population of the bentonite. The ABM tests showed that the equilibrium cation population may depend on the bentonite type and locally different conditions. They, therefore, provide a unique chance to study the range of cation populations that result from saturation with a specific water composition. This equilibrium cation population is represented by average EC values (not considering the contact).

In all three ABM experiments so far, the most stable observation is strong modification of $EC_{population}$ while CEC values decreased only slightly (Table 4):

- Average exchangeable $Mg^{2+}_{(av. \ 1-8 \ cm)}$ values decreased by 17% (ABM-1), 60% (ABM-2), and 12% (ABM-5).
- Average exchangeable $Na^+_{(av. \ 1-8 \ cm)}$ values decreased by 19% in ABM-1 and 55% in ABM-2, but was more or less unchanged on average with +1% in ABM-5.
- Average exchangeable $Ca^{2+}_{(av. \ 1-8 \ cm)}$ values increased by 41% (ABM-1), ~200% (ABM-2), and 21% (ABM-5).
- Average $CEC_{(av. \ 1-8 \ cm)}$ values decreased slightly by 5.5 meq $100 \ g^{-1}$ in ABM-1 and 1.8 meq $100 \ g^{-1}$ in both ABM-2 and ABM-5.

Differences in the equilibrium EC values were not only found between the different ABM tests but also within the individual tests, i.e. in various segments of the ABM packages. One of the reasons was fractures in the host rock supplying the blocks with groundwater, as discussed by Wallis et al. (2016) for ABM-1. Here, fractures supplied the package with groundwater in the upper part, resulting in a decrease in exchangeable Na^+ and an increase in exchangeable Ca^{2+} in this part (Table 4). In ABM-2 where water saturation was technically difficult as water pressure dropped during the heating phase indicating possible boiling (Dohrmann et al., 2017), the situation was even more complicated. Water, on the other hand, was also distributed by the sand between the package and rock wall (Eng et al., 2007), causing a large excess of ECs (cf. also Svensson et al., 2023). In ABM-5, all groundwater inflow probably came from one fracture located 0.8 m down from the floor (Svensson et al., 2023) with the consequence that in ABM-5 more exchangeable Ca^{2+} was present in this part.

The described differences are from *in situ* experiments in a crystalline rock laboratory at repository depth (Äspö), and conditions were much more realistic than in batch experiments with respect to water/rock ratio and static *versus* dynamic conditions allowing gradients in the material to form over time. Water was always present during heating, which differs markedly from oven-drying experiments as discussed recently by Kaufhold et al. (2023a). Water-contents measurements after termination, on the other hand, did not always show full water saturation in long-term heater experiments (e.g. Fernández et al., 2018,
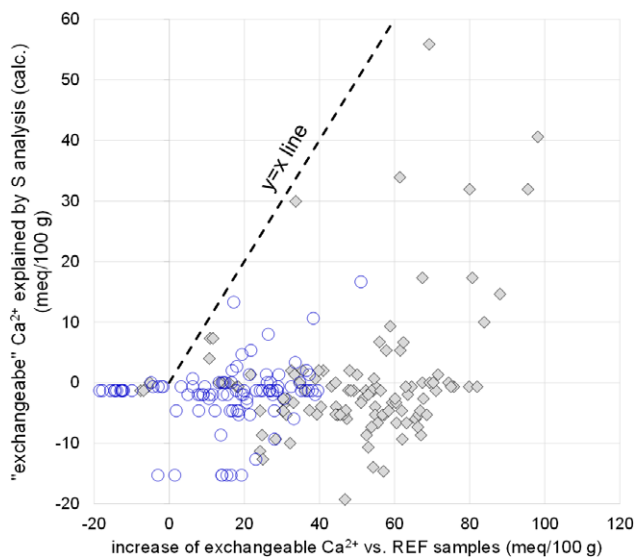
Figure 9. Correlation between the measured increases in exchangeable Ca^{2+} values and the calculated 'exchangeable Ca^{2+}' values from anhydrite and gypsum dissolution. Data from ABM-5 (open circles, n=101) and ABM-2 (diamonds, n=116).

Table 4. Observed differences between the ABM-1, ABM-2, and ABM-5 samples.

parameter	ABM–1	ABM–2	ABM–5
heating	from start	after water saturation	after water saturation
duration of heating phase	1 year	3–4 years	4+7 months
max. temperature	140°C	140°C	132°C + 250°C
artificial water saturation by Ti tubes	4 holes per block (120 in total)	4 holes each 10 blocks	4 holes at bottom, not used
Na-Ca-Cl-SO$_4$ dominated groundwater (Svensson et al., 2023)	~2470 mg/L Na$^+$	~2470 mg/L Na$^+$	~1600 mg/L Na$^+$
	~2560 mg/L Ca^{2+}	~2560 mg/L Ca^{2+}	~760 mg/L Ca^{2+}
	~8580 mg/L Cl$^-$	~2560 mg/L Cl$^-$	~3970 mg/L Cl$^-$
	~480 mg/L SO$_4^{2-}$	~480 mg/L SO$_4^{2-}$	~330 mg/L SO$_4^{2-}$
groundwater inflow from fractures in crystalline rock	upper part	complex	lower part
No. of blocks	30	31	30
horizontal gradient (Na$^+$)	-	upper part	whole parcle
horizontal gradient (Mg^{2+})	-	upper part	lower+upper part
horizontal gradient (Ca^{2+})	-	-(inflated)	lower part
horizontal gradient (CEC)	-	-	upper+middle part
Na$^+$ loss/gain (total)	−19%	−55%	+1%
Mg^{2+} loss (total)	−17%	−60%	−12%
Ca^{2+} gain (total)	41%	ca. 200%	21%
Na$^+$ loss (section)	upper part	middle part	lower+upper part
Mg^{2+} loss (section)	-	upper part	whole parcle
Ca^{2+} gain (section)	upper part	upper part	whole parcle
CEC drop (average)	−5.5 meq/100 g	−1.8 meq/100 g	−1.8 meq/100 g
CEC drop	9 different bentonites	MX80 (4x). Asha	FEBEX
sum-CEC average	<+5 meq/100 g	ca. +20 meq/100 g. partly inflated	+7 meq/100 g
Cl$^-$	large scale equilibrium	large-scale equilibrium, partly inflated	large-scale equilibrium, increased
SO$_4^{2-}$	not analyzed	inflated (anhydrite, gypsum)	no evidence
boiling	-	assumed	possibly
Na+/Mg^{2+}-ratio reacted	3.1 (blocks 16–30); 2.9 (blocks 1–15)	5–10 (blocks 16–31); 3.5 (blocks 1–15)	2–15 (blocks 21–30); 2–6 (blocks 12–20); 2–17 (blocks 1–11)
REF samples ratio %/CEC	Na 48:Mg 18:Ca 32	Na 54:Mg 17:Ca 29	Na 45:Mg 22:Ca 33
equilibrium ratio %/CEC (finally)	Na 39:Mg 15:Ca 45	Na 27:Mg 7:Ca "100"	Na 46:Mg 10:Ca 54
ratios of how many blocks?	*n*=12	*n*=29	*n*=30

full-scale engineered barrier experiment (FEBEX); Svensson et al., 2023, ABM experiments). Small-scale variations in water contents with wet and dry parts may be local driving forces for geochemical and mineralogical alteration. All these factors come into play when differences in ECs and CECs are discussed between different *in situ* heater experiments.

Differences in terms of the EC$_{population}$ evolution may result from different heating/saturation processes. The duration of the heating phase was similar in ABM-1 and ABM-5 (11 and 12 months) with similar exchangeable Mg^{2+} losses; however, other factors also varied such as maximum temperature ranging from 140°C (ABM-1, ABM-2) up to 250°C (ABM-5), plus temperature gradients in all heater experiments both from heater to rock side as well as along the packages. Heating also started either from the very beginning

(installation, ABM-1) or after water saturation (ABM-2, ABM-5) monitored by relative humidity sensors. The next important parameter for EC and CEC changes is the water saturation with water coming from fractures in the crystalline rock and, to a greater or lesser extent, from an artificial water saturation system with much more water supply in ABM-1 > ABM-2 > ABM-5. The same source as natural groundwater was used for the artificial water saturation system.

As exchangeable Ca^{2+} values were partially inflated in ABM-2, the other two major cations were used to find out if an equilibrium EC$_{population}$ may have formed during *in situ* tests with similar buffer materials: Na$^+$/Mg^{2+} ratios were useful to understand homogeneous EC variations of the entire length of an ABM package. In ABM-1 these ratios were relatively constant (~3) and less constant in ABM-2 with

Na$^+$/Mg^{2+} ratios in the same range in the lower half, but higher ratios in the upper half due to the assumed boiling processes causing local evaporation with halite formation. At much higher temperatures in ABM-5, the ratio also varied much more in the vertical direction of the package in the upper and lower parts. In the middle part, Na$^+$/Mg^{2+} ratios came close to those observed in ABM-1 and ABM-2. Aside from local disturbances, a general trend of Na$^+$/Mg^{2+} ratios (≈ 3) possibly to reach an equilibrium was observed in all three ABM experiments analyzed, allowing modelers to adjust variable parameters such as selectivity coefficients (Bruggenwert and Kamphorst, 1981; Wallis et al., 2016).

The parameter CEC, which in bentonites mainly originates from smectites, is no absolute property of that material. CECs are measured by extraction experiments over relatively short times (minutes to hours) using index cations that are able to replace naturally occurring cations present on exchange sites. Other experimental conditions such as electrolyte concentration are also factors that may result in different CEC values (cf. Dohrmann, 2006b; Dohrmann et al., 2012b). In practical daily work, robust comparable CECs and ECs can be obtained for bentonites when carefully analyzed using even different index cations (cf. Dohrmann

and Kaufhold, 2009; Dohrmann et al., 2012a; Dohrmann et al., 2012b). Keeping this in mind, a closer evaluation of the observed CEC differences at various distances from the heater showed that increasing temperatures decreased the CEC values in ABM-5 (Fig. 10). On average, however, CEC losses were small (1.8 meq 100 g^{-1}, 30 blocks; Table 4). Different slopes and visual inspection showed that the CECs are significantly lower at the contact point with the heater (Fig. 10a), with a less pronounced loss also at 1 cm from the heater (Fig. 10b). At 5 cm and 8 cm almost no CEC decrease of reacted samples was observed. Any possible CEC decrease could have resulted from: (1) structural degradation of the smectites; (2) collapse of the interlayer and fixation of cations resulting in a '0 water layer' arrangement with limited CEC properties; (3) 'dilution' of the sample by the precipitation of secondary minerals, with low CEC values; or (4) by pH changes affecting variable charges caused either by pH of inflowing water or even by cation exchange (Kaufhold et al., 2008).

A significant CEC $_{(av.\ 1–8\ cm)}$ decrease over an entire block volume, however, was only observed for Febex (9 meq 100 g^{-1}, block #13), a bentonite that is known for partial fixation of exchangeable cations with formally 8% illitic layers in its R0 I-S
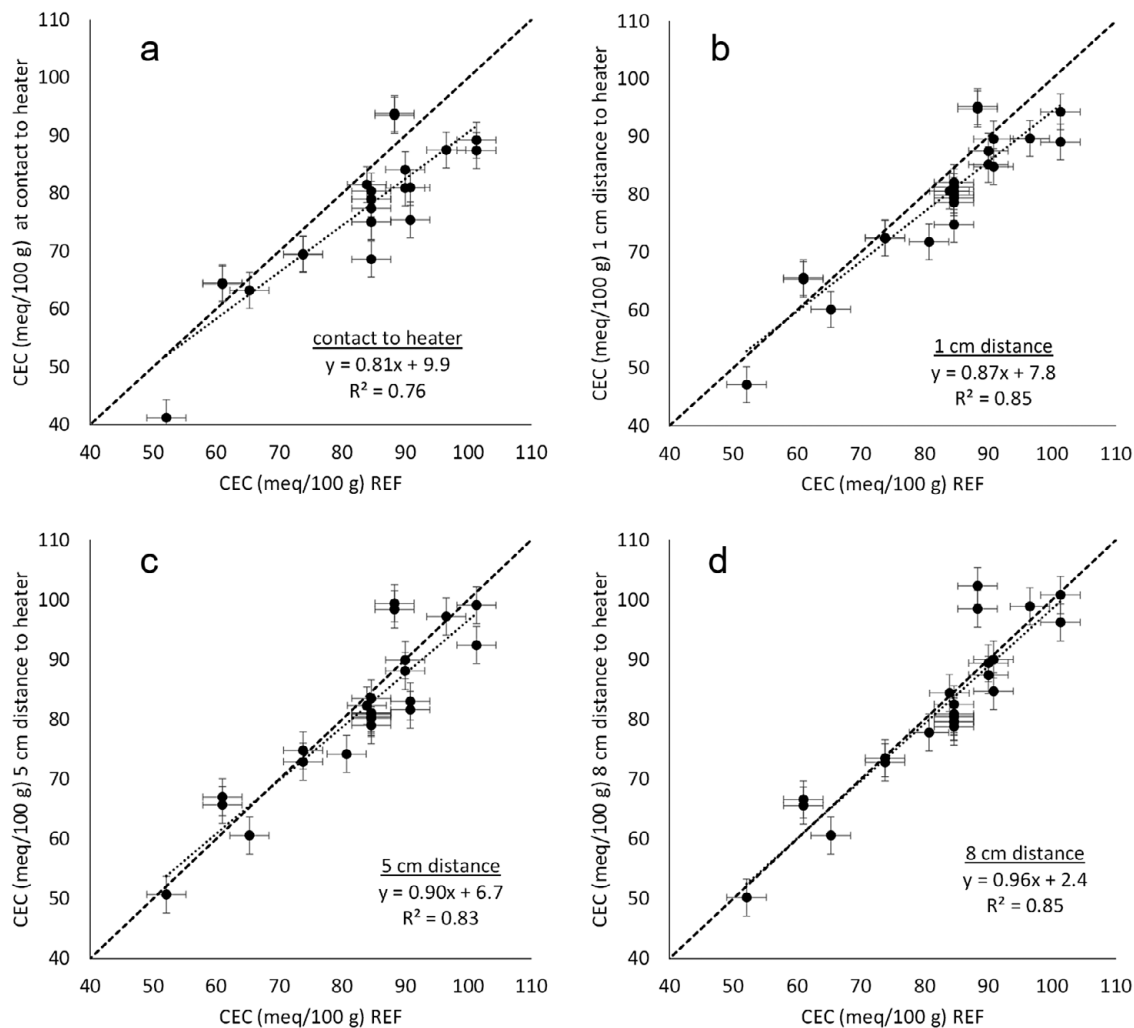
Figure 10. CEC differences relative to REF samples observed at various distances from the heater: (a) bentonites in direct contact with heater; (b) bentonites at a distance of 2 cm distance from the heater; (c) bentonites at a distance of 5 cm from the heater; and (d) bentonites at a distance of 8 cm from the heater. Note that error bars represent ±3 sigma ($n=4$). 'Contact' bentonite samples may be diluted by corrosion products possibly reducing CEC values.

structure (Fernández et al., 2018). These so-called illitic layers may also be characterized as a smectitic '0 water' layer (0w layer) arrangement and consequently without the necessary larger layer charge of illitic layers (cf. Ferrage et al., 2005; Ufer et al., 2012). During a CEC extraction experiment, cations in such 0w layer arrangements (collapsed interlayer regions) may not be hydrated and replaced (Kaufhold et al., 2023b), indicating a loss in swelling capacity under the conditions of a CEC experiment. Real illitization, however, requires replacement of structural Si atoms by Al, increasing the charge of the structural 2:1 unit of platelets on both sides of the interlayer region, including exchangeable or fixed cations. Such a phenomenon was not observed by XRD at least in the contact samples that were analyzed by Kaufhold et al. (2021).

As discussed for ABM-5, the same average CEC drop was observed for the ABM-2 experiment heated to a much lower maximum temperature of 140°C (Table 4), but a much stronger CEC drop of, on average, 5.5 meq 100 g^{-1} was reported for the nine different blocks with CEC index cation data studied in ABM-1 (Dohrmann et al., 2013b). In the present experiment, an important difference may have been that heating started immediately after installation, while in ABM-2 and ABM-5 sensor data were used to detect full water saturation after several months, and heating started afterward. In ABM-2 and ABM-5 altogether, CEC dropped in only three different bentonite materials (MX80, Asha 505, and Febex). The major difference in ABM-1 was a much lower water content of bentonite materials (8.2–16.8% water; Svensson et al., 2011) when heating started, which is closer to real repository conditions where canisters packed with heat-producing waste are brought into contact with bentonite buffer and where heating would start without any delay for water saturation as forced in ABM-2 and ABM-5.

Partial drying of block materials was observed at larger temperatures (ABM-5) and as a consequence of the assumed boiling and partial fracturing (ABM-2) as reported by Svensson et al. (2023). Here, the water content of reacted block materials varied between 11 and 43% (ABM-2) and 11 and 31% (ABM-5). Looking more closely at the data, a differentiation can be made for ABM-2 below and above the fractured zone (with assumed boiling). Here, in all pure bentonite blocks at >29 mm from the heater, the water contents were well above 25%. Directly above this fractured zone in Asha 505 (#21) a CEC drop of 7 meq 100 g^{-1} was measured, while the second Asha 505 block (#10) a few blocks lower showed insignificant CEC decrease of 2 meq 100 g^{-1}. Calcigel just below the fractured zone (#18) had a minor CEC increase (3 meq 100 g^{-1}) and a minor CEC decrease of 1 meq 100 g^{-1} far away from that zone (#3). No conclusion can be drawn from these few examples with respect to the assumption that drying starting from high water content of ~30% would reduce CEC values significantly in *in situ* experiments. On the other hand, when blocks with small water contents (8.2–16.8%; Svensson et al., 2011) were heated from the start, CEC values showed a greater decrease of, on average, 5.5 meq 100 g^{-1} in ABM-1 (Dohrmann et al., 2011). All the bentonite blocks had water contents of ~30% after the experiment; only Kunigel V1 had between 20 and 25% water (Svensson et al., 2011). One observation may be of importance for future studies: in the two bentonite ABM-1 blocks with the lowest initial exchangeable Na$^+$ content of 1% Na$^+$/CEC (Rokle #13) and 3% (Calcigel #23), the CEC decrease was the smallest (2.7 and 1.1 meq 100 g^{-1}). All other analyzed blocks had between 27 and 94% Na$^+$/CEC and lost 3.7–8.8 meq 100 g^{-1} of the REF CECs.

Future studies of the ABM-3 experiment will allow this hypothesis to be verified because that package was installed for a much longer time at similar temperatures to those for ABM-1, and ABM-3 was heated from the start. If CEC decreases are related to dry heating and a starting EC$_{population}$ of >~25% Na$^+$/CEC, such a systematic CEC decrease should also be present in the reacted materials of ABM-3.

Cl⁻ uptake and distribution over the entire ABM-5 package

The chloride anion is regarded as being excluded from smectitic interlayer positions in highly compressed bentonite blocks as long as the remaining water is preferentially interlayer water (e.g. Tournassat and Appelo, 2011; Tournassat et al., 2016).

In the literature, most studies reported results from *in situ* experiments in crystalline rock in contact with high saline groundwater. In contrast to such studies, the bentonites installed in the Febex experiment had contact with low-saline groundwater. The bentonite itself contained chloride in the pore water and this chloride moved towards the heater during the experiment (Fernández et al., 2018). The authors detected secondary chloride mineral phases in this part, which means that care has to be taken when using bulk chloride data and not chloride data from pore-water extracts. The amounts reported in studies with very saline groundwater, on the other hand, are relatively large and most of the bulk chloride may be chloride in pore water. In some parts of ABM-2, halite was possibly the result of boiling and evaporation (Svensson et al., 2023). Halite, however, would also be dissolved using aqueous extracts.

Keeping this in mind, chloride concentrations before and after all ABM experiments showed the following characteristics: 'the most Cl⁻-rich bentonites/clays (Asha 505, Friedland, and Ikosorb) display a loss in chloride, whereas the other bentonites have gained chloride during the field test', as reported already for ABM-1 on 11 analyzed blocks (Svensson et al., 2011). The same distribution was observed for ABM-2 (Dohrmann et al., 2017) and ABM-5 (this study), with even larger amounts of chloride by a larger uptake of groundwater. Obviously, chloride is able to move over long distances in such heater experiments and is present all over the highly compacted materials, not only close to the sand filters outside the blocks in the gap towards the host rock which were applied to distribute the water to the blocks. In four of five blocks studied in ABM-5, chloride concentrations increased including the chloride-rich REF material of Febex bentonite (#25), and 'the content is lower at the heater contact (H) than at the granite contact (G)' (Fernández et al., 2022). In the high-temperature heater experiment (maximum temperature 140°C) called LOT-A2, chloride concentrations increased in four sampled blocks to concentrations half way between Äspö groundwater and the initial pore-water concentration of the MX80 bentonite used (Karnland et al., 2009). In the low-temperature real-scale heater experiment referred to as the 'prototype repository', chloride was found to increase in all the bentonite samples in both No. 5 and No. 6 deposition holes with greater contents in blocks that were water saturated (Olsson et al., 2013). In the other real-scale experiment referred to as 'TBT', chloride increased in the horizontal direction from the rock to the heater (Åkesson, 2012), but no specified data on concentrations were published in the reports. In summary, chloride is typically taken up by groundwater saturating the bentonite, and at elevated temperatures (85–250°C), chloride was found all over all blocks after the experiment of usually a few months to several years.
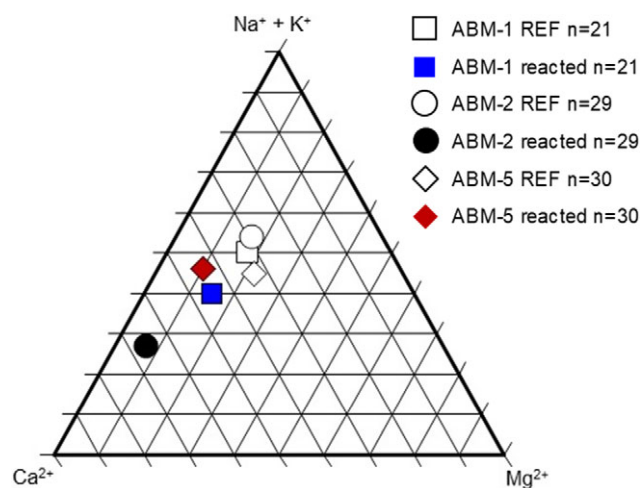
Figure 11. Modification of the $EC_{population}$ of buffer blocks used in ABM experiments. Note that in ABM-1 only 21 of 30 blocks were used for calculation of the average values whereas in ABM-2 and ABM-5 (nearly) all blocks were analyzed. In ABM-2, the Ca^{2+} per cent values of reacted blocks were inflated by the presence of sulfates and Ca^{2+} per cent values were reduced from '100%' to 66% to give a sum of 100% for all exchangeable cations to be visible in a triplot figure. The position of the filled circle in reality is closer to the '100%' Ca^{2+} edge.

Variation of the CECs and the ECs on a larger horizontal and vertical scale

To obtain a quick overview of the changes in $EC_{population}$, averages of all single blocks were calculated, resulting in a single data point in a triangle with the dominant cations (Fig. 11). ABM-2 (29 blocks) and ABM-5 (30 blocks) are the only heater experiments with a more or less full set of analyses of all blocks that could be sampled for analysis of the $EC_{population}$. ABM-1 also had 21 analyzed blocks, which allowed comparison of average values of the REF composition and final (reacted materials) composition in a single data point, each (Fig. 11). The REF sample ratios of %/CEC for ABM-1 were Na 48: Mg 18:Ca 32 and ended up in a ratio with much less Na and Mg on exchange sites: Na 39:Mg 15:Ca 45. REF composition was very similar for ABM-2 and ABM-5; the reacted samples, however, were all much closer to the '100%' Ca^{2+} edge of the diagram (Fig. 11). Note that in ABM-2 Ca^{2+} percentage values of reacted blocks were inflated by the presence of sulfates, and Ca^{2+} percentage values were reduced from '100%' to 66% to give a sum of 100% for all exchangeable cations to be visible in a triplot figure. The position of the filled circle in reality is closer to the '100%' Ca^{2+} edge. ABM-5 ended relatively parallel to the '100%' Na^+ edge. Obviously, at such high temperatures, selectivity changed in a way that exchangeable Na^+ can compete successfully for exchange positions, although care has to be taken because the Na^+/Ca^{2+} ratio of the groundwater was more Na^+-rich in ABM-5 (Na^+/Ca^{2+} ratio ≈ 2:1) compared with ABM1-3 (Na^+/Ca^{2+} ratio ≈ 1:1), and based on the available data, this influence on $EC_{population}$ cannot be distinguished from temperature effects.

Summary and conclusions

EC measurements are needed to follow the early reactions in bentonite buffer experiments subjected to heat and water uptake in *in situ* experiments. Compared with the former ABM-1 and ABM-2, in ABM-5 more pronounced horizontal gradients, both of CEC and EC, were detected after heating to 250°C.

The equilibria between exchangeable cations as observed for ABM-1 and -2 were also different, particularly for the stable average

concentration of exchangeable Na^+ in ABM-5. The open question is, if these differences could have been controlled by a greater Na^+/Ca^{2+} ratio ≈ 2:1 in the inflowing water. ABM-5 could be an exercise for future studies on less heated ABM-4 analyzed after retrieval saturated with the same groundwater.

Cl^- is believed to be excluded from the interlayer of smectites, at least in the compacted state in which the interlayer is not supposed to form >2w layers. Nevertheless, a significant uptake of Cl^- was observed in all ABM tests and in many other *in situ* experiments at Äspö which derived from inflowing water and migrated possibly through low density domains in the compacted bentonite.

In comparison with the lower temperature ABM-1 experiment, more or less stable CEC values (only minor decreases) were detected. A driving force for the greater CEC decrease of ABM-1 may have been that bentonite blocks with small amounts of water and a starting average $EC_{population}$ of >~25% Na^+/CEC, before saturation with groundwater, were heated as would be the case in a realistic application in a repository for heat producing HLRW. Future studies of the ABM-3 experiment will allow verification of this hypothesis because ABM-3 was also heated from the start and the duration will be much greater.

Overall, different values for $EC_{population}$ of the different ABM tests were found which cannot yet be explained. The most likely reasons are different water saturation/heating processes and different compositions of the inflowing groundwater. Nevertheless, all bentonites in all tests approached an apparent equilibrium interlayer composition which can be characterized by a range of Na^+ (27–46%/CEC), Mg^{2+} (7–15%/CEC), and Ca^{2+} (45–100%/CEC).

References

Åkesson, M. (2012). *Temperature Buffer Test, Final Report*. SKB technical report, TR-12-04, Stockholm, Sweden. https://www.skb.com/publication/2447163/TR-12-04.pdf

Arcos, D., Bruno, J., Benbow, S., & Takase, H. (2000). *Behaviour of Bentonite Accessory Minerals During the Thermal Stage*. SKB technical report, TR-00-06, Stockholm, Sweden. Available online at: https://www.skb.com/publication/17397/TR-00-06.pdf

Bildstein, O., & Claret, F. (2015). Stability of clay barriers under chemical perturbations. In *Handbook of Clay Science, Techniques and Applications* (ed. F. Bergaya and G. Lagaly), pp. 155–188. Elsevier, Amsterdam. https://doi.org/10.1016/B978-0-08-100027-4.00005-X

Bruggenwert, M.G.M., & Kamphorst, A. (1981). Survey of experimental information on cation exchange in soil systems. In *Soil Chemistry*

B. Physico-Chemical Models, 2nd edn (ed. G.H. Bolt, editor), pp. 141–203. Elsevier, Amsterdam.

Brusewitz, A.M. (1986). Chemical and physical properties of Palaeozoic potassium bentonites from Kinnekulle, Sweden. *Clays and Clay Minerals*, *34*, 442–454.

Dohrmann, R. (2006a). Cation Exchange Capacity Methodology III: correct exchangeable calcium determination of calcareous clays using a new silver-thiourea method. *Applied Clay Science*, *34*, 47–57.

Dohrmann, R. (2006b). Cation exchange capacity methodology I: An efficient model for the detection of incorrect cation exchange capacity and exchangeable cation results. *Applied Clay Science*, *34*, 31–37.

Dohrmann, R., & Kaufhold, S. (2009). Three new, quick CEC methods for determining the amounts of exchangeable calcium cations in calcareous clays. *Clays and Clay Minerals*, *57*, 338–352.

Dohrmann, R., & Kaufhold, S. (2010). Determination of exchangeable calcium of calcareous and gypsiferous bentonites. *Clays and Clay Minerals*, *58*, 513–522.

Dohrmann, R, Genske, D., Karnland, O., Kaufhold, S., Kiviranta, L., Olsson, S., Plötze, M., Sandén, T., Sellin, P., Svensson, D., & Valter, M. (2012a). Interlaboratory exchange of CEC and exchangeable cation results of bentonite buffer material. I. *Cu(II)-triethylenetetramine method.* Clays and Clay Minerals, *60*, 162–175.

Dohrmann, R., Genske, D., Karnland, O., Kaufhold, S., Kiviranta, L., Olsson, S., Plötze, M., Sandén, T., Sellin, P., Svensson, D., & Valter, M. (2012b). Interlaboratory exchange of CEC and exchangeable cation results of bentonite buffer material. *II. Alternative methods.* Clays and Clay Minerals, *60*, 176–185.

Dohrmann, R., Kaufhold, S., & Lundqvist, B. (2013a). The role of clays for safe storage of nuclear waste. In *Handbook of Clay Science, Techniques and Applications* (ed. F. Bergaya and G. Lagaly), pp. 677–710. Elsevier, Amsterdam.

Dohrmann, R., Olsson, S., Kaufhold, S., & Sellin, P. (2013b). Mineralogical investigations of the first package of the alternative buffer material test – II. *Exchangeable cation population rearrangement.* Clay Minerals, *48*, 215–233.

Dohrmann, R. & Kaufhold, S. (2014). Cation exchange and mineral reactions observed in MX 80 buffers samples of the prototype repository in situ experiment in Äspö, Sweden. *Clays and Clay Minerals*, *62*, 357–373.

Dohrmann, R., & Kaufhold, S. (2017). Characterization of the second package of the alter-native buffer material experiment (ABM) – II. Exchangeable cation population rearrangement. *Clays and Clay Minerals*, *65*, 104–121.

Dueck, A., Johannesson, L.-E., Kristensson, O., & Olsson, S. (2011). *Report on Hydro-Mechanical and Chemical-Mineralogical Analyses of the Bentonite Buffer in Canister Retrieval Test*. SKB technical report TR-11-07, Stockholm, Sweden. http://skb.se/upload/publications/pdf/TR-11-07.pdf

Eng, A., Nilsson, U., & Svensson, D. (2007). *Äspö Hard Rock Laboratory, Alternative Buffer Material Installation Report IPR-07-15*, Stockholm, Sweden. http://skb.se/upload/publications/pdf/ipr-07-15.pdf

Faucher, J.A., Southworth, R.W., & Thomas, H.C. (1952). Adsorption studies on clay minerals. I. *Chromatography on clays*. Journal of Chemical Physics, *20*, 157–160. https://doi.org/10.1063/1.1700160

Fernández, A.M., Kaufhold, S., Sanchez-Ledesma, D.M., Rey, J.J., Melon, A., Robredo, L.M., Fernandez, S., Labajo, M.A., & Clavero, M.A. (2018). Evolution of the THC conditions in the FEBEX in situ test after 18 years of experiment: smectite crystallochemical modifications after interactions of the bentonite with a C-steel heater at 100℃. *Applied Geochemistry*, *98*, 152–171.

Fernández, A.M., Marco, J.F., Nieto, P., León, F.J., Robredo, L.M., Clavero, M.Á., Cardona, A.I., Fernández, S., Svensson, D., & Sellin, P. (2022). Characterization of bentonites from the in situ ABM5 heater experiment at Äspö Hard Rock Laboratory, Sweden. *Minerals*, *12*, 471.

Ferrage, E., Lanson, B., Sakharov, B.A., & Drits, V.A. (2005). Investigation of smectite hydration properties by modeling experimental X-ray diffraction patterns: Part I. Montmorillonite hydration properties. *American Mineralogist*, *90*, 1358–1374.

Gaines G.L., & Thomas H.C. (1953). Adsorption studies on clay minerals. II. A formulation of the thermodynamics of exchange adsorption. *Journal of Chemical Physics*, *21*, 714–718. https://doi.org/10.1063/1.1698996

Jacobsson, A., & Pusch, R. (1978). *Egenskaper hos bentonitbaserat buffertmaterial*. KBS Teknisk rapport 1978-06-10. https://www.skb.com/publication/2910/

Johannesson, L.-E., Börgesson, L., Goudarzi, R., Sandén, T., Gunnarsson, D., & Svemar, C. (2007) Prototype repository: a full-scale experiment at Äspö HRL. *Physics and Chemistry of the Earth*, *32*, 58–76.

Karnland, O., Sandén, T., Johannesson, L.-E., Eriksen, T.E., Jansson, M., Wold, S., Pedersen, K., Mutamedi, M., & Rosborg, B., (2000). *Long Term Test of Buffer Material. Final Report on the Pilot Parcels*. SKB technical report, TR-00-22, Stockholm, Sweden. https://www.skb.se/upload/publications/pdf/TR-00-22.pdf

Karnland, O., Olsson, S., Dueck, A., Birgersson, M., Nilsson, U., & Hernan-Håkansson, T. (2009). *Long Term Test of Buffer Material at the Äspö Hard Rock Laboratory, LOT Project*. SKB technical report TR-09-29, Stockholm, Sweden. https://www.skb.com/publication/1961944/

Kaufhold, S., Dohrmann, R., Koch, D., & Houben, G. (2008). The pH of aqueous bentonite suspensions. *Clays and Clay Minerals*, *56*, 338–343.

Kaufhold, S., Dohrmann, R., Sandén, T., Sellin, P., & Svensson, D. (2013). Mineralogical investigations of the alternative buffer material test – I. Alteration of bentonites. *Clay Minerals*, *48*, 199–213.

Kaufhold, S., Sanders, D., Hassel, A.-W., & Dohrmann, R. (2015). Corrosion of high-level radioactive waste iron-canisters in contact with bentonite. *Journal of Hazardous Materials*, *285*, 464–473.

Kaufhold, S., & Dohrmann, R. (2016). Assessment of parameters to distinguish suitable from less suitable high-level-radioactive waste bentonites. *Clay Minerals*, *51*, 289–302.

Kaufhold, S., Dohrmann, R., Götze, N., & Svensson, D. (2017a). Characterization of the second parcel of the alternative buffer material (ABM) experiment – I. Mineralogical reactions. *Clays and Clay Minerals*, *65*, 27–41.

Kaufhold, S. Dohrmann, R., & Gröger-Trampe, J. (2017b). Reaction of native copper in contact with pyrite and bentonite in anaerobic water at elevated temperature. *Corrosion Engineering, Science and Technology*, *52*, 349–358.

Kaufhold, S., Dohrmann, R., Ufer, K., Svensson, D., & Sellin, P. (2021). Mineralogical analysis of bentonite from the ABM5 heater experiment at Äspö Hard Rock Laboratory, Sweden. *Minerals*, *11*, 669. https://doi.org/10.3390/min11070669

Kaufhold, S., Dohrmann, R., Wallis, I., & Weber, C. (2023a). Chemical and mineralogical reactions of bentonites in geotechnical barriers at elevated temperatures – review of experimental evidence and modelling progress. *Clay Minerals*, *58*, 280–300.

Kaufhold, S., Dohrmann, R., & Gröger-Trampe, J. (2023b). About the possibility to liberate naturally present fixed cations from dioctahedral smectites by hydrothermal treatment. *Applied Clay Science*, *244*, 107115

Kosec, T., Qin, Z., Chen, J., Legat, A., & Shoesmith, D.W. (2015). Copper corrosion in bentonite/saline groundwater solution: effects of solution and bentonite chemistry. *Corrosion Science*, *90*, 248–258.

Kumar, S.R., Podlech, C., Grathoff, G., Warr, L.N., & Svensson, D. (2021). Thermally induced bentonite alterations in the SKB ABM5 hot bentonite experiment. *Minerals*, *11*, 1017. https://doi.org/10.3390/min11091017

Kumpulainen, S., & Kiviranta, L. (2011). *Mineralogical, Chemical and Physical Study of Potential Buffer and Backfill Materials from ABM Test Package 1*. Posiva Working Report 2011–41. Posiva Oy, Olkiluoto, Finland. http://www.iaea.org/inis/collection/NCLCollectionStore/_Public/43/068/43068661.pdf .

Kumpulainen, S., Kiviranta, L., & Korkeakoski, P. (2016). Long-term effects of Fe-heater and Äspö groundwater on smectite clays – chemical and hydromechanical results from *in-situ* alternative buffer material (ABM) test package 2. *Clay Minerals*, *51*, 129–144.

Meier, L.P., & Kahr, G. (1999). Determination of the cation exchange capacity (CEC) of clay minerals using the complexes of copper (II) ion with triethylenetetramine and tetraethylenepentamine. *Clays and Clay Minerals*, *47*, 386–388.

Müller-Vonmoos, M., Kahr, G., Bucher, F., & Madsen, F.T. (1990). Investigation of Kinnekulle K-bentonite aimed at assessing the long-term stability of bentonites under repository conditions. *Engineering Geology*, *28*, 269–280.

Müller-Vonmoos, M., Kahr, G., & Madsen, F. (1994). Intracrystalline swelling of mixed-layer illite-smectite in K-bentonites. *Clay Minerals*, *29*, 205–213.

Neretnieks, I. (1978). *Transport of Oxidants and Radionuclides Through a Clay Barrier*. Kungl Tekniska Högskolan Stockholm 1978-02-20. https://www.skb.com/publication/2962/TR79webbNY_OCR.pdf

Olsson, S., & Karnland, O. (2011). Mineralogical and chemical characteristics of the bentonite in the A2 test parcel of the LOT field experiments at Äspö HRL, Sweden. *Physics and Chemistry of the Earth*, *36*, 1545–1553.

Olsson, S., Jensen, V., Johannesson, L.-E., Hansen, E., Karnland, O., Kumpulainen, S., Svensson, D., Hansen, S., & Lindén, J. (2013). *Prototype Repository. Hydromechanical, Chemical and Mineralogical Characterization of the Buffer and Backfill Material from the Outer Section of the Prototype Repository.* SKB technical report TR-13-21, Stockholm, Sweden. https://www.skb.com/publication/2477824

Pusch, R. (1983). *Stability of Deep-Sited Smectite Minerals in Crystalline Rock – Chemical Aspects.* SKB technical report TR-83-16, Stockholm, Sweden. https://www.skb.com/publication/3114/

Samper, J., Naves, A., Montenegro, L., & Mon, A. (2016). Reactive transport modelling of the long-term interactions of corrosion products and compacted bentonite in a HLW repository in granite: uncertainties and relevance for performance assessment. *Applied Geochemistry*, 67, 42–51.

Sandén, T., Goudarzi, R., Combarieu, M., Åkesson, M., & Hökmark, H. (2007). Temperature buffer test – design, instrumentation and measurements. *Physics and Chemistry of the Earth*, 32, 77–92.

Sandén, T., Nilsson, U., Andersson, L., & Svensson, D. (2018). *ABM45 Experiment at Äspö Hard Rock Laboratory.* Installation Report. SKB Rep. P-18-20. https://www.skb.com/publication/2491709/P-18-20.pdf

Savage, D. (2011). A review of analogues of alkaline alteration with regard to long-term barrier performance. *Mineralogical Magazine*, 75, 2401–2418.

Sellin, P., & Leupin, O. (2014). The use of clay as an engineered barrier in radioactive waste management – a review. *Clays and Clay Minerals*, 61, 477–498.

Shimbashi, M., Yokoyama, S., & Sato, T. (2024). Review of secondary phases formed under natural alkaline conditions at low temperatures and implications for cement–bentonite interactions in radioactive waste repositories. *Clays and Clay Minerals*, 72, e2, 1–16

SKB (2007). RD&D Programme 2007. *Programme for Research, Development and Demonstration of Methods for the Management and Disposal of Nuclear Waste.* SKB technical report TR-07-12, Stockholm, Sweden. http://www.skb.se/upload/publications/pdf/TR-07-12_FUD_2007_eng_webb.pdf

Stanjek, H., & Künkel, D. (2016). CEC determination with Cu-triethylenetetramine: recommendations for improving reproducibility and accuracy. *Clay Minerals*, 51, 1–17.

Sun, Z., Chen, Y., & Ye, W. (2022). A systematic review of bentonite/concrete interaction system in HLW disposal repositories: theoretical, experimental and geochemical modelling analysis. *Construction and Building Materials*, 353, 129075

Svensson, D., Dueck, A., Nilsson, U., Olsson, S., Sandén, T., Lydmark, S., Jägerwall, S., Pedersen, K., & Hansen, S. (2011). *Alternative Buffer Material. Status of the Ongoing Laboratory Investigation of Reference Materials and Test Package 1.* SKB technical report TR-11-06, Stockholm, Sweden. http://skb.se/upload/publications/pdf/TR-11-06.pdf

Svensson, D., Bladström, T., Sandén T., Dueck A., Nilsson U., & Jensen, V. (2023). *Alternative Buffer Material (ABM) Experiment. Investigations of Test Packages ABM2 and ABM5.* SKB technical report TR-23-25, Stockholm, Sweden. http://skb.se/upload/publications/pdf/TR-23-25.pdf

Szakálos, P., & Seetharaman, S. (2012). *Corrosion of Copper. Technical Note 201217.* ISSN: 2000-0456.

Tournassat, C., & Appelo, C.A.J. (2011). Modelling approaches for anion-exclusion in compacted Na-bentonite. *Geochimica et Cosmochimica Acta*, 75, 3698–3710.

Tournassat, C., Bourg, I., Holmboe, M., Sposito, G., & Steefel, C.I. (2016). Molecular dynamics simulations of anion exclusion in clay interlayer nanopores. *Clays and Clay Minerals*, 64, 74–388.

Ufer, K., Kleeberg, R., Bergmann, J., & Dohrmann, R. (2012). Rietveld refinement of disordered illite-smectite mixed layered structures by a recursive algorithm. I: One-dimensional patterns. *Clays and Clay Minerals*, 60, 507–534. https://doi.org/10.1346/CCMN.2012.0600507

Wallis, I., Idiart, A., Dohrmann, R., & Post, V. (2016). Reactive transport modelling of groundwater-bentonite interaction: effects on exchangeable cations in an alternative buffer material in-situ test. *Applied Geochemistry*, 73, 59–69.

Wersin, P. & Birgersson, M. (2014). Reactive transport modelling of iron–bentonite interaction within the KBS-3H disposal concept: the Olkiluoto site as a case study. In *Geological Society, London, Special Publications 2014*, vol. 400, pp. 237–250. doi: 10.1144/SP400.24

Wersin, P., Jenni, A., & Mäder, U.K. (2015). Interaction of corroding iron with bentonite in the ABM1 Experiment at Äspö, Sweden: a microscopic approach. *Clays and Clay Minerals*, 63, 51–58.

Zheng, L., Rutqvist, J., Birkholzer, J.T., & Liu, H.H. (2015). On the impact of temperatures up to 200 °C in clay repositories with bentonite engineer barrier systems: a study with coupled thermal, hydrological, chemical, and mechanical modelling. *Engineering Geology*, 197, 278–295. https://doi.org/10.1016/j.enggeo.2015.08.026